Summer 2010

The mitigation effects of a barrier wall on blast wave pressures

Nathan Thomas Rouse

Department:

THE MITIGATION EFFECTS OF A BARRIER WALL ON BLAST WAVE PRESSURES

By

NATHAN THOMAS ROUSE

A THESIS

Presented to the Faculty of the Graduate School of the

MISSOURI UNIVERSITY OF SCIENCE AND TECHNOLOGY

In Partial Fulfillment of the Requirements for the Degree

MASTER OF SCIENCE IN EXPLOSIVES ENGINEERING

2010

Approved by:

Jason Baird, Advisor
Paul N. Worsey
Kwame Awuah-Offei

ABSTRACT

The study examined the mitigating effects of a blast barrier wall. This area of blast mitigation is of interest due to the many different applications involved in protecting a specific target from an explosive attack. The research follows a 1:50 scale layout using 73 gram, hemisphere-shaped, Composition-4 charges detonated at combinations of three standoff distances from a blast barrier wall set at three different heights. This project used 45 data points for each combination of standoff distance and wall height. This project expanded prior research conducted by the United States Army Corps of Engineers (USACE) by increasing the database of recorded pressures behind a barrier wall and finding that a barrier wall creates an elongated effect on the pressure reduction area behind the wall. In other words, the pressure reduction area extends more along the wall than it does away from the wall.

The results of further study indicate how and to what extent the wall affects the pressures created by the detonation of the Composition-4 hemispheres in the regions selected. The distance at which the blast pressures were mitigated was affected by the wall height and standoff distance. The wall height had a greater impact on the extent of the percent pressure reduction than did the standoff distance; however, the standoff distance has the greatest effect on the magnitude of the pressures behind a barrier wall.

In the end, it is hoped that the analysis contained in this thesis will aid in future investigations of blast barrier walls and lead to more in-depth analyses and the creation of more complex models to predict the effects of blast barrier walls on detonation shocks and pressures from charges detonated at finite distances from the walls.

ACKNOWLEDGEMENTS

I thank my advisors and professors in the Mining Engineering Department, Dr. Jason Baird, Dr. Paul Worsey, and Dr. Kwame Awuah-Offei, for providing mentoring and advice on explosives and data analysis for this project. In addition, the work of Phil Mulligan was invaluable in obtaining and setting up the blast table at the beginning of this project. I also thank Jim Taylor and DeWayne Phelps for their help and support at the Experimental Mine.

I am grateful for the financial support I have received, and I particularly wish to thank Barb Robertson and Shirley Hall for their help in obtaining this support.

Finally, I appreciate the support of my friends and family, and I thank The Grotto for enabling me to make it through one more year of school.

TABLE OF CONTENTS

LIST OF ILLUSTRATIONS

Page

LIST OF TABLES

Page

1. INTRODUCTION

Blast barrier walls can be used to mitigate explosive damage to target structures that would otherwise be harmed by a blast from the detonation of an explosive charge. Barrier walls serve two purposes in this instance:

1. They ensure that an explosive charge is set at a standoff distance away from a protected object.
2. Up to a point, they diffract blast waves to mitigate the full force of the blast pressures on the protected object.

This project is concentrated more with the latter purpose than the former; however, both purposes are addressed by the analysis outlined by this report. It is an investigation of the factors that affect the performance of a barrier wall against the effects of air blast and provides empirical data and analysis that can facilitate the design of an effective blast barrier wall. This analysis is important in that it will provide an idea for a simple empirical model to aid in the design of a blast barrier wall and address multiple ways the wall can aid in blast mitigation. The results will be useful to the U.S. Department of State, the U.S. Department of Energy, the U.S. Department of Defense, and civilian nuclear power stations that must protect facilities from vehicle bomb threats or any other mobile explosive threat. Additionally, the data collected can be used to help complete neural network software tools used in blast mitigation design and analysis.

For this research, various wall heights, explosive standoff distances, and data point locations were used to record the pressures created by explosive charges. Pressure transducers were located at various angles to an imaginary axis intersecting the charge

locations and the center point of the barrier wall (Figure 1.1). The transducers were located on the opposite side of the wall from the charge positions at specified angles to the axis. The data recorded by the pressure transducers were compared using charts and graphs of the pressures, scaled distances, and data point locations.

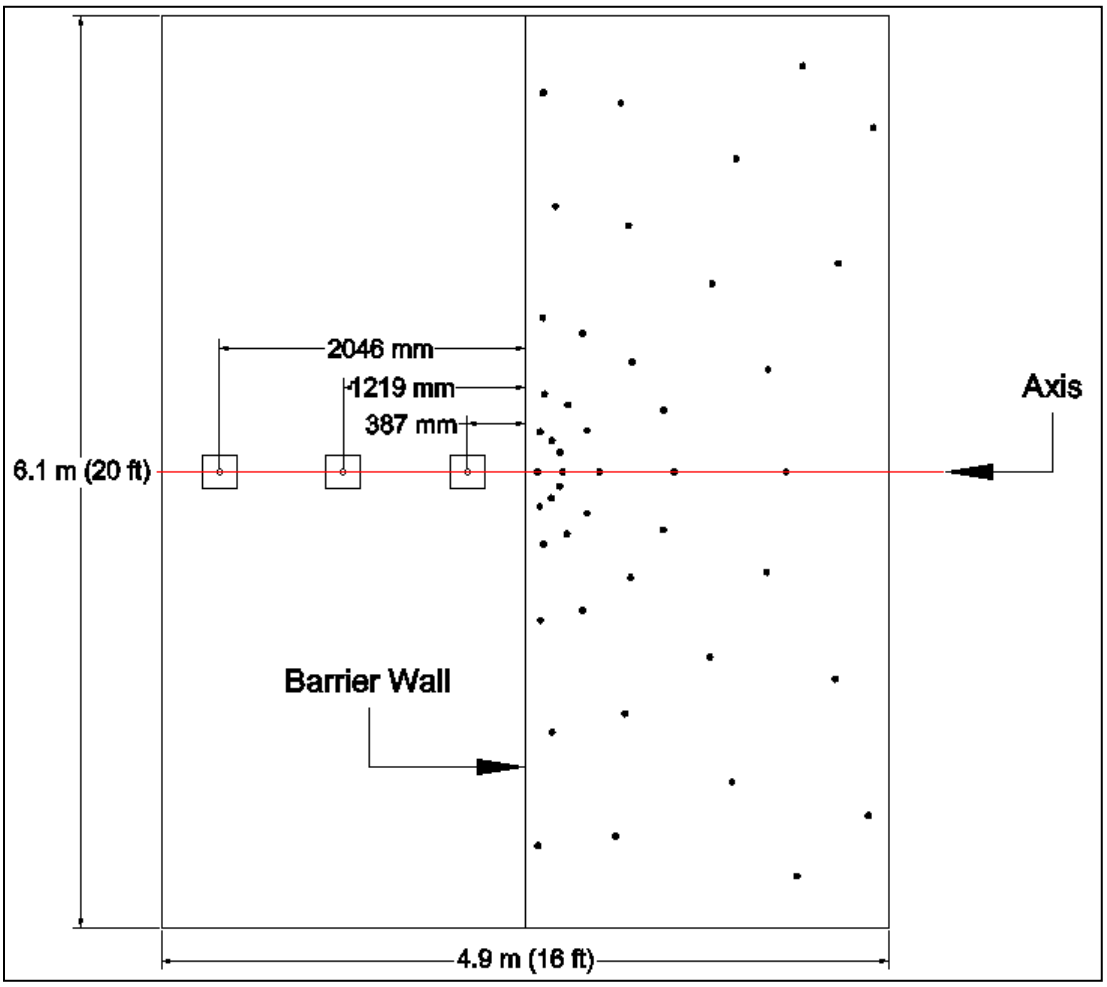

Figure 1.1. Blast table with charge and pressure recording locations.

The tests conducted in this project explored the effects of a blast barrier wall on an explosive pressure wave using experiments with a 1:50 scale setup. The scale up

simulates a 9,071 kg (20,000 lb) Composition-4 charge at standoff distances of 19.2 m, 61.0 m, and 102.4 m (63 ft, 200 ft, and 336 ft) and barrier wall heights of 3.7 m and 11.3 m (12 ft and 37 ft). This size of charge simulates a box truck or water/fuel truck bomb scenario (Figure 1.2). The scaled setup included the charge size, barrier wall height, and distances at which the pressures were recorded. The barrier wall tests were conducted on a large steel blast table at the Missouri University of Science and Technology (Missouri S&T) Experimental Mine. This blast table is similar to one at the United States Army Corps of Engineers' (USACE) Geotechnical and Structures Laboratory, which was used by researchers to produce the report upon which this project builds (Rickman and Murrell, 2004). That report offers three recommendations for future research. The present work addressed each of the three:

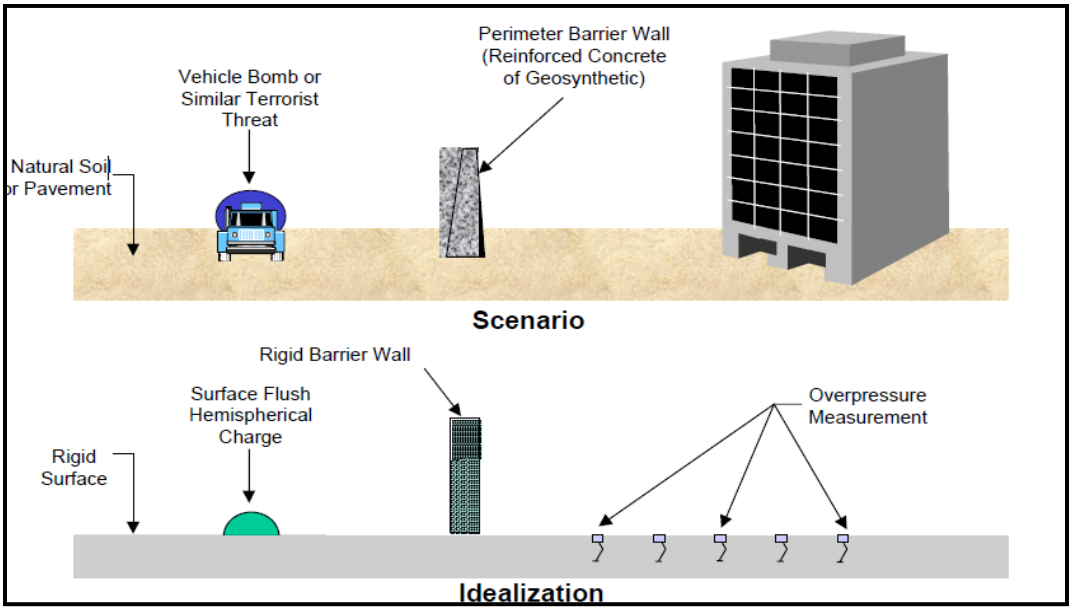

Figure 1.2. Test Scenario (Rickman and Murrell, 2004).

analysis of the off-axis pressure locations, expansion of the database of recorded pressures, and evaluation of the shielded area. It also analyzed the relationship between the barrier wall height and standoff distance and the effect the two parameters had on the area behind the barrier wall.

Primarily, this thesis does more than just expand on the research produced by the USACE. Most importantly, the data was used to determine the extent of the area of influence behind the barrier wall where the blast pressures are most affected by the wall. This area was then studied to determine the individual factors that had the greatest effect. Additionally, the health benefits of reducing the pressures were also reviewed since a reduction in blast pressures at locations protected by barrier walls could equal a reduction in fatality and/or injury rates.

2. REVIEW OF LITERATURE

For many years, structures have undergone blast loads due to large-scale blasts. These large-scale blasts were caused by devices ranging from terrorist devices and conventional explosive charges to nuclear weapons. For example, 5.5 tons of explosives in a vehicle bomb were detonated at the U.S. Marine Corps Battalion Headquarters in Beirut in 1983. Over 300 people were killed or wounded in the attack, which demolished the concrete building in contact with the vehicle. In 1984, in Antilias, East Beirut, 2.8 tons of explosives were used to attack the U.S. Embassy Annex. In this case, the car bomb was detonated on a sunken road approaching the Annex car park, and a small retaining wall provided some shielding to the blast at a standoff distance from the embassy. Due to the barrier wall, the casualty rate was relatively low and only 11 deaths were recorded (Smith and Hetherington, 1994). These two contrasting scenarios give some idea of how important blast barrier walls can be in situations involving explosive attacks.

To understand how a blast pressure wave interacts with a barrier wall, one must first understand a free-field blast pressure wave. The supersonic detonation within a high explosive forms gases which undergo violent expansion. This expansion causes the surrounding layer of air to compress and form a blast wave. The blast wave which follows the detonation shock wave is a high pressure wavefront that expands out from the explosive charge. It is followed by a negative pressure trough before the air resumes its natural equilibrium at atmospheric pressure (Johansson and Persson, 1970 and Smith and Hetherington, 1994).

For this project, the pressure wave is formed by a hemispherical charge on the table surface. The shock front that the charge produces travels along the surface of contact and expands outward from the charge into the atmosphere. In a free-field application, this blast wave propagates along the surface until it is no longer supersonic. It behaves this way until a structure, such as a barrier wall, is introduced. The barrier wall in this project simulates a blast interaction with a large target. The blast wave from a charge at some standoff distance impacts the barrier wall, which, due to its size and construction does not move. This causes the blast wave to diffract over the barrier wall (Figure 2.1). The wave is reduced for some distance behind the barrier wall before that distance becomes large enough that the pressures are no longer affected by the wall (Smith and Hetherington, 1994 and Remennikov and Rose, 2007). The area where the wall affects the blast pressures and causes a pressure reduction is defined as the shadow area. The extent of this shadow area defines the effectiveness of the barrier wall with respect to pressure reduction. This is the effect of blast barrier walls that was investigated by the research leading to this thesis.

The effect of barrier walls on blast pressures has been studied prior to this investigation. The Army Corps of Engineers' Geotechnical and Structures Laboratory published a report on research conducted on a blast table using Composition-4 (C-4) explosive charges, and various wall heights and standoff distances (Rickman and Murrell, 2004). It is from the USACE report that this study primarily draws for experimental setup and procedure. The USACE investigated how the pressures produced by an explosive charge were affected by a blast barrier wall and the effectiveness of the ConWep program in predicting the pressure reduction caused by the barrier wall.

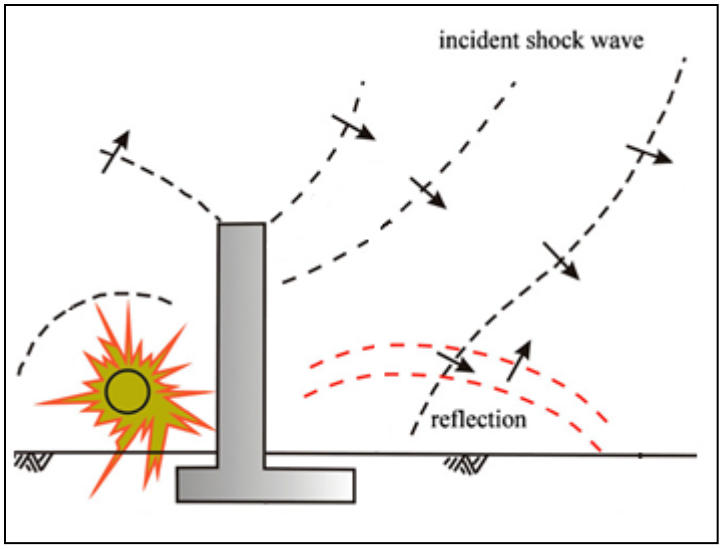

Figure 2.1. Blast wave diffraction over a barrier wall (Remennikov and Rose, 2007).

ConWep software is used to calculate blast effects of conventional weapons, and in the case of the USACE report, it can effectively calculate blast pressures and pressure reduction caused by a barrier wall. ACE also concluded that the maximum effect of the barrier wall was produced at the smallest standoff distance and largest wall height.

The USACE report suggested that off-axis pressure locations be analyzed, that the database of recorded pressures be expanded, and that the shielded area be evaluated. These recommendations were evaluated and are included in this study.

ConWep, the conventional weapons effects software created and maintained by the USACE Protective Design Center, was not used for this study; however, the USACE suggests that it can be used to predict the peak pressures produced over a barrier wall. ConWep is based on charts in Army Technical Manual (TM) 5-855-1, *Fundamentals of Protective Design for Conventional Weapons*, which contains information on structural response to conventional weapons. Another technical manual, TM 5-853-3, *Security*

Engineering Final Design, contains methods for calculating pressures and impulses behind a barrier wall; however, the circulation of these technical manuals is restricted and both have limited availability (Remennikov and Rose, 2007). The software that was available for use was the Blast Effects Computer (BEC), which is a program developed by the U.S. Department of Defense Explosives Safety Board to aid in predicting blast pressures from explosive devices for magazine site and storage evaluations based on the casing, composition, and size of the device, as well as the explosion site and the atmospheric conditions. The macro-enabled Microsoft Excel © spreadsheets in the BEC calculate the TNT equivalence, scaled distance, time of arrival, over-pressure, reflected pressure, impulse, duration, window breakage probability, eardrum rupture probability, and lethality probability due to lung damage (Blast Effects Computer, 2001). This program was used in this project to predict the pressures produced by the 73 gram charge and to successfully check that the 1:50 scale-up to a 20,000 lb charge would produce similar pressures at the scaled-up distances.

Other than within the USACE, there have been many studies on effects of blast pressures on structures. The work of Remennikov and Rose (2007) addresses the use of empirical data and neural networks to predict the area of effect of a blast barrier wall on structures behind a wall. It investigated how a blast wave is affected by a barrier wall and examined the physical changes that a blast wave undergoes by using an artificial neural network. The advantage of artificial neural networks is in their speed. Predicting blast effects could take hours using computational fluid dynamics (CFD) programs; however, artificial neural networks combine results from tests and from CFD model runs into data sets, and only take minutes to complete an analysis. Through empirical data, the

Remennikov and Rose study shows that the use of neural networks is a feasible option to predicting pressures behind a barrier wall.

Zhou and Hao (2006) also describe the blast loading of structures behind a barrier wall. Their study introduced formulae based on empirical results of pressures on a rigid wall behind a barrier to predict peak reflected pressure and impulse. These formulas can be used together with TM-1300, *Structures to Resist the Effects of Accidental Explosions*, to estimate the impulse and pressure on buildings behind a barrier wall. The majority of studies based on barrier wall research, such as those described, determine pressures on structures behind a blast wall; however, they do little to study the barrier wall's effect on a blast wave without the interference of structures or how blast waves are affected by a barrier to cause loads on structures behind the barrier. A study of a barrier wall's effect on a blast wave would help to fully understand the area of pressure reduction due to a barrier wall and how a barrier wall affects the blast pressure on the horizontal plane.

Walter (2004) describes the process of measuring air blasts and details how to properly use a pressure transducer. The article depicts how an explosive waveform progresses and shows the difference between incident pressure, free-field pressure, and reflected pressure. It explains that incident pressure and free-field pressure are synonymous and describe the pressure created by an expanding shock wave. When the free-field wave reflects from a surface, it creates a reflected pressure wave. Two types of pressure transducers are used to measure these waves. Side-on transducers are used to measure free-field pressures without interfering with the flow behind the shock wave, while reflected-pressure transducers (such as those used in this study) are used to measure reflected pressures at normal incidence to a rigid surface. This type of

transducer must be mounted flush to that surface. Walter's document was used to define the pressures that were of interest to this thesis research and aid in selecting the proper pressure transducers for the experiment.

Two methods of scaling were used in this study, scaled distance and charge weight scaling. This thesis research used scaled distance in order to compare calculations with the scaled distance in the USACE report. Smith and Hetherington (1994) and Cooper (1996) provide the definition, identification, and use of scaled distance. Scaled distance can be described by more than one formula; however, and the most used formula is the Hopkinson-Cranz model. This model, described by Smith et. al. as the ratio of distance to the charge over the third root of the charge weight, was used by the USACE investigation. The second use of scaling, charge weight scaling, was used to calculate the size of the corresponding full-scale explosive charge based on the charge from the 1:50 scale experiments. When scaling up the size of an explosive charge to gain the equivalent scale-up of pressure, the charge mass must be scaled correctly (Cooper, 1996). Mass is based on volume; therefore, scaling mass is based on scaling the volume of the charge. Since volume scales proportionally with respect to the cube of the scaling factor, charge mass is also proportional to the cube of the scaling factor (i.e., to calculate the full-scale charge size, the 1:50 scale model must be multiplied by 50^3.).

One major importance of blast barrier walls is the reduction of casualty rates due to the standoff distance and effects on blast pressure created by a barrier wall. Pressure levels that relate to certain critical organ failures in people differ depending on the documentation; therefore there is a wide variability in pressure levels cited and their relation to the reaction of the human body. TM 1300 states that the eardrum damage

threshold is at 5 psi overpressure, the lung damage threshold is at 30 to 40 psi overpressure, and the lethality threshold is at 100 to 120 psi overpressure. Near 100% lethality occurs at 200 to 250 psi overpressure (TM 1300, 1990). Zipf, et al. agree with the pressures that invoke eardrum rupture; however, they state that the lung damage threshold is at 15 psi overpressure, and that the fatality threshold is at 35 to 45 psi overpressure. They also state that nearly 100% lethality occurs at 55 to 65 psi overpressure (Zipf, R and Cashdollar, K, 2007). The similarity between the lung damage threshold of TM 1300 and fatality threshold of Zipf, et. al. may be that lung damage is a significant enough injury to cause death due to gas release from agitated alveoli of the lungs (TM 1300). One aspect of blast waves that has a great effect on tissue is the impulse, which was not studied in this project. Impulse is the integral of the pressure versus time curve; therefore it is a function of the pressure and the time over which the pressure has an effect on an object. As impulse increases, the tolerance of tissue or structures to pressure decreases. The longer tissue or structures is affected by a blast wave, the pressure the tissue or structure can withstand decreases (Zipf and Cashdollar, 2007). This thesis uses the more conservative numbers of Zipf, et al. in its analysis of blast effects on human tissue damage and fatality rate.

3. EXPERIMENTAL PROCEDURE

3.1. EQUIPMENT

The data acquisition phase of this project took place at the Missouri S&T Experimental Mine. The mine property is the location of all outdoor explosive testing at Missouri S&T, and is also the site of the explosive storage magazines. The Experimental Mine was chosen for this series of tests because it is large enough to house the blast table (Figure 3.1), which had to be located outdoors due to the nature of the experiments and the availability of the site; proximity to the magazines is very convenient.

Figure 3.1. Free-field setup of the blast table with a 73 gram charge at a 387 mm standoff distance.

3.1.1. Blast Table. The 6 m by 4.9 m (20 ft by 16 ft) steel table comprised three separate sections (Figure 3.1). One side of the table contained three ignition areas, one for each of the three standoff locations of the explosive charges. The opposite side of the table had 111 pre-constructed data acquisition points radiating from the center point of the barrier wall to the edges of the table. The final section was the blast barrier wall, which could be raised as high as 0.8 m (32 in) above the plane of the table.

The data collection points were positioned in radiating arcs from the center point of the wall opposite the points of detonation (Figure 3.2). The table had seven expanding arcs of data points at distances of 8.4 cm, 24.9 cm, 49.8 cm, 100.0 cm, and 175.1 cm (3.3 in, 9.8 in, 19.6 in, 39.4 in, and 68.9 in) from the wall. The seven rows of arcs, from innermost to outermost, consisted of 15 points, 17 points, 19 points, 19 points, 19 points, 16 points, and 6 points. Due to restrictions on the size of the experiments, data acquisition system limitations, and to keep the sample size, costs, and time within manageable limits, only 45 sample points out of a total of 111 possible points were used. Arc 1 consisted of one sample point, arc 2 consisted of seven sample points, arc 3 consisted of seven sample points, arc 4 consisted of nine sample points, arc 5 consisted of nine sample points, arc 6 consisted of eight sample points, and arc 7 consisted of four sample points. The data acquisition system records up to 16 channels of data at once; therefore, three layouts of pressure transducers were enough to cover the 45 chosen sample points.

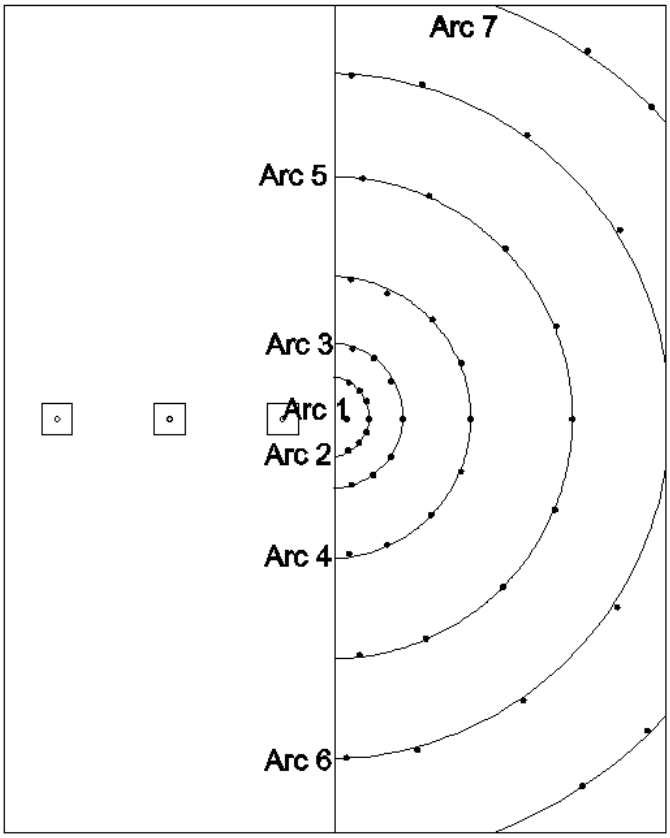

Figure 3.2. Blast table depicting seven arcs of sample points.

Forty-five points were chosen instead of utilizing the full 48 available points that could have been recorded by the data acquisition system to keep with the intent to use every other sample point on the table. Also, the three extra channels were kept open in the event that one of the channels on the data acquisition system ceased to work properly. If one channel began to malfunction, only 45 possible samples could be recorded. This strategy prevented the project from unwanted downtime due to unpreventable problems with the data acquisition system, such as a software or hardware malfunction.

The sample points were chosen such that the final data would yield as much information as possible on the pressures affected by the barrier wall while demanding the

fewest possible test iterations. The 45 sample points represented less than 50% of the available data points; however, the sample point layout was designed to ensure that all critical data was gathered by analyzing the entire table equally in all areas without looking in-depth in any one region. If an in-depth analysis was required in any one region, further testing could be completed to analyze that specific area.

Three standoff points were used in the blast table tests at distances of 387 mm, 1219 mm, and 2046 mm (15.25 in, 48 in, and 80.6 in) from the wall. The use of various standoff distances was intended to indicate the extent to which a blast wave is affected by the barrier wall when the charge was placed at different locations with respect to the wall (Figure 3.3).

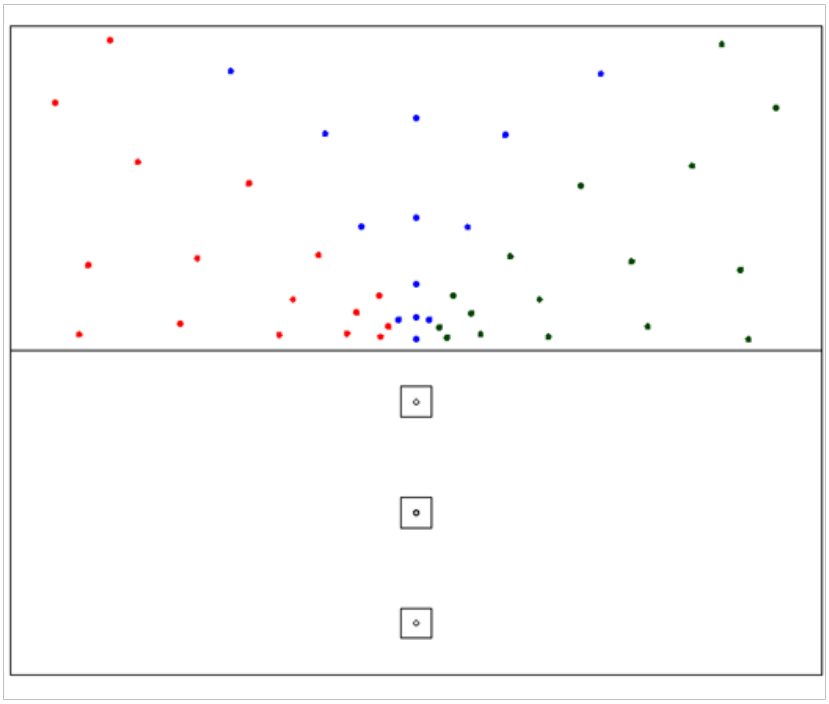

Figure 3.3. Plan view of the blast table with the three sample point layouts shown by different colors.

The center point of each arc of transducer locations was on a line that passed through the center of each blast location; that line was also perpendicular to the blast wall. This line, which was deemed the 0 degree line, was used to identify the location of data points at an angle to the axis (Figure 3.4). Therefore, the points were located by degree of the angle to the axis (not by degree of the angle to the wall).

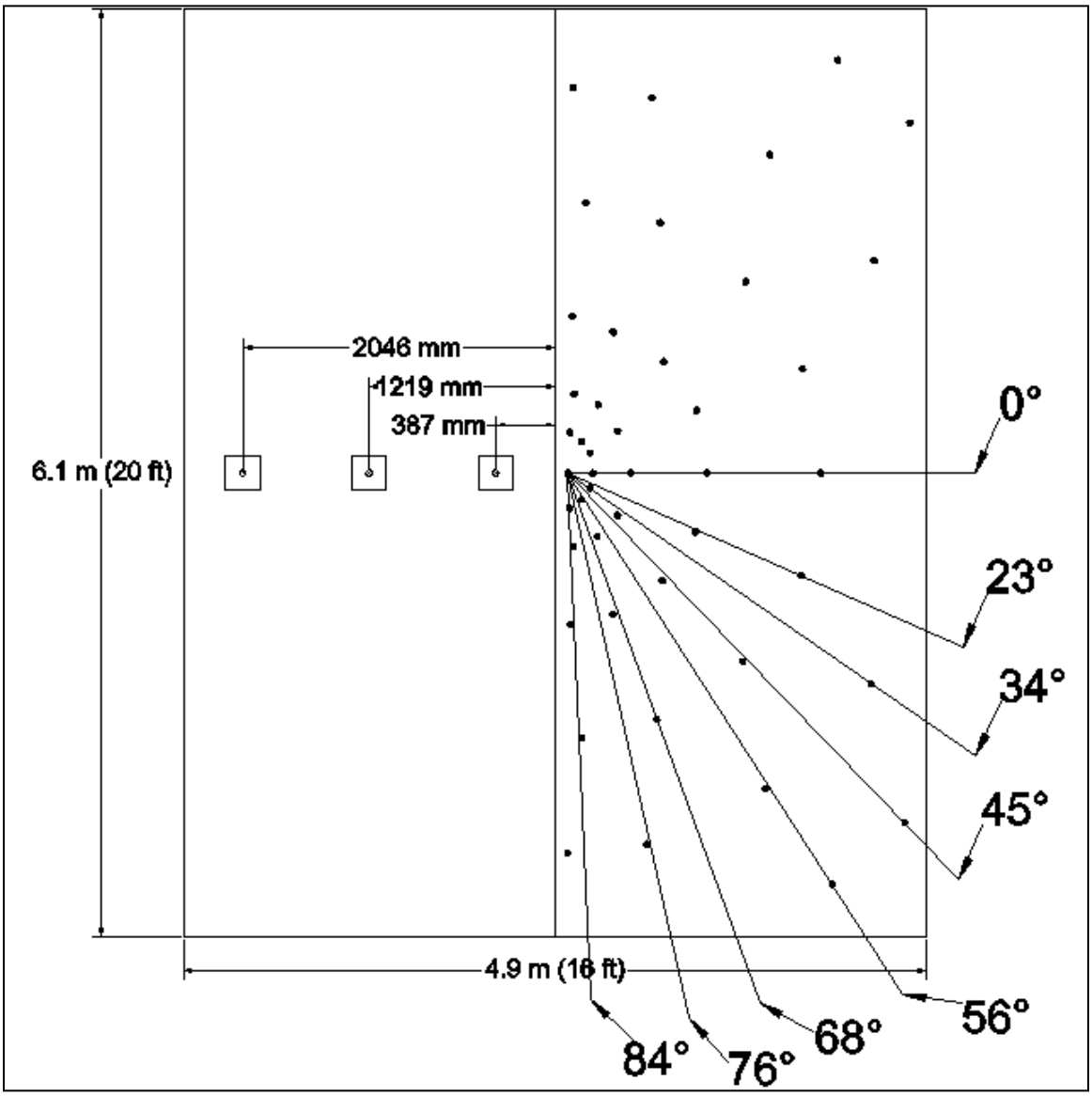

Figure 3.4. Blast table with dimensions and angles.

3.1.2. Pressure Transducers. Three models of high-resolution, PCB Integrated Circuit-Piezoelectric pressure transducers (PCB Piezotronics, Inc, Depew, NY) were utilized to determine the reflected pressure along the surface of the rigid table. An important feature of the PCB transducers is they are integral-electronics piezoelectric (IEPE) gages, which convert output from the transducer to a low impedance signal, eliminating noise effects, and permitting the use of inexpensive cables that do not require noise treatment. The pressure transducers were PCB Piezotronics Models 102B, 102B04, and 102B15. Each transducer was calibrated for the expected pressure produced at its location based on the results of the models in the Blast Effects Computer (Department of Defense Explosives Safety Board, 2001). Model 102B can accurately measure pressures ranging from 1 to 5000 psi; Model 102B04 can accurately measure pressures ranging from 0.2 to 1000 psi; Model 102B15 can accurately measure pressures ranging from 0.05 to 200 psi.

3.1.3. Data Acquisition System. The Synergy Data Acquisition System (DAS) (Hi-Techniques, Inc, Madison, WI) is a portable device incorporating signal conditioning, a computer, memory, and a computer software package that was used in this project in its oscilloscope mode to record the pressures created by each test (Figure 3.5). The DAS can record up to 16 channels at once; thus, it dramatically reduced the number of tests required by allowing 16 data points to be recorded for each shot. The important attribute of this software/hardware package is that the Synergy DAS also has universal signal conditioning incorporated into its software so that amplifiers were not required to boost the signal from the pressure transducers to the DAS. Also, the data recorded during the experiments could be saved to the hard drive for later analysis.

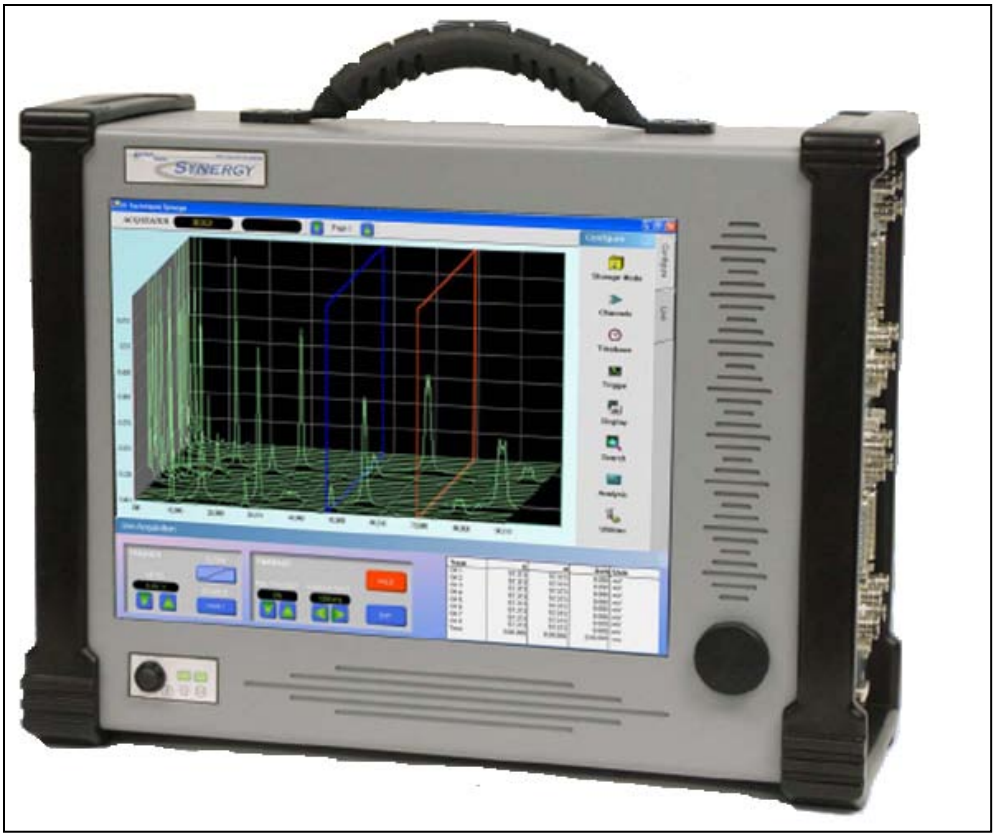

Figure 3.5. Synergy DAS

3.2. SETUP

Each test was set up using one of three layouts of pressure transducers, one of three standoff distances, and one of three wall heights to keep the experimental setup simple. The charge size and geometry were kept uniform. This was done to minimize experimental error associated with any inconsistencies in the setup of the experiments. Any variation in these factors could have potentially caused the pressures to behave differently from one test to another.

3.2.1. Blast Table. The wall height of the blast table can be adjusted from 0 mm (0 in) to 813 mm (32 in). Only three wall heights were chosen for this experiment: a

height of 0 mm was used for free-field tests to calibrate the table for comparison with tests completed previously by the USACE (Rickman and Murrell, 2004) and to identify the blast wave pattern without any obstruction. Barrier wall heights of 73 mm (2.9 in) (Figure 3.6) and 226 mm (8.9 in) (Figure 3.7) were also chosen from among the six used in the USACE tests. These wall heights were chosen from the USACE tests so that the results could be compared between the two sites using identical wall heights, and the chosen heights represent a broad view of the effects that the barrier wall height can have on pressure reduction.

Figure 3.6. Blast table with wall height of 73 mm.

Figure 3.7. Blast table with wall height of 226 mm.

As noted in Section 3.1.1., three standoff distances were utilized in this project. Each position consisted of a cut-out in the blast table, and a removable square steel plate. The steel plates fit into the table cut-out, and a flange under the table around each cut-out supported each plate. For each test in this experiment, the steel plate at the charge location was replaced with a cardboard square to support the explosive charge, and each square was drilled through the center with a ¼ in drill bit to create a location for placement of a Dyno Nobel #1 MS Series Masterdet electric detonator (Figure 3.8).

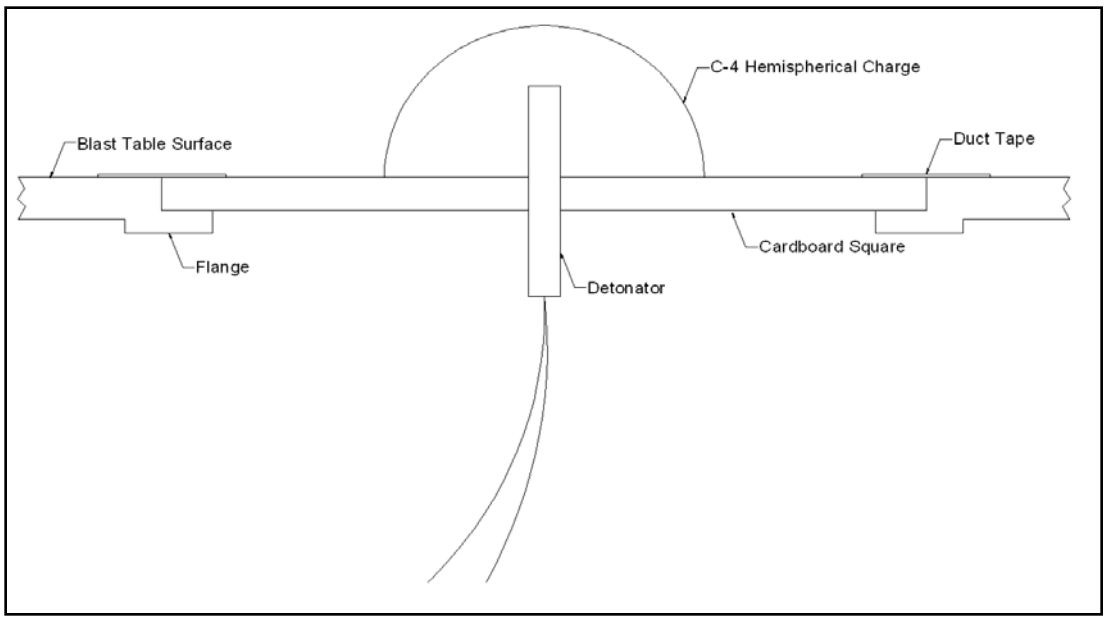

Figure 3.8. Charge setup (not to scale).

The steel squares were replaced because they were more expensive than cardboard squares and cost time to manufacture since they were useful for only a single test. The cheap cardboard squares were easy to use as a replacement material for the square plates. To examine the quality of the results when using a cardboard square, a test was conducted using sample points along the axis and the free-field setup (Table 3.1).

During these tests, it was found that the steel plates spalled and damaged the concrete foundation of the blast table. Also, as Table 3.1 shows, the difference in pressures produced between tests using plates made of steel and cardboard is significant enough to include an average adjustment. The average of the percent difference of steel and cardboard for the five locations is 15%. The pressures produced using cardboard plates on the blast table at Missouri S&T were increased by the 15% average to match results that would be expected from using steel plates.

Table 3.1. Comparison between steel and cardboard plates
(The point column matches with sample point locations described in Figure 3.9.)

Point	Pressures using Steel (psi)	Pressures using Cardboard (psi)	% Difference of Steel and Cardboard
8	118.690	105.371	11%
24	59.848	57.174	4%
42	37.365	27.659	26%
61	15.943	13.224	17%
80	6.611	5.491	17%

3.2.2. Pressure Transducers. The pressure transducers were screwed into the table from underneath until they were flush with the top of the blast table to minimize disturbance in pressure readings. Then the transducers were connected to the Synergy DAS by coaxial cables, which were inspected for any kinking that could have damaged the cable or insulation or induced noise and disturbance in the pressure readings. Due to the number of data points required for each combination of wall height and standoff distance, testing was conducted using three separate transducer arrays. Table 3.2 and Figure 3.9 match each transducer to its sample point location for each of the three arrays. The points can be matched to the experimental results found in the Appendix. Figure 3.9 only shows the 45 sample points that were used in these tests; however, the labeling convention includes all 111 points that are available for use on the table. The points were labeled in this manner throughout the experiment because they weren't physically identified on the table. Keeping the layout uncomplicated like this was the easiest way to ensure the correct sample points were used for every test.

Table 3.2. Pressure transducer models and locations.

Model	Serial	Point relating to Figure 3.8		
		Array 1	Array 2	Array 3
102B	29322	18	8	28
102B	29323	20	22	30
102B	29324	35	24	45
102B	29325	37	26	47
102B	29327	39		49
102B04	29178	53		65
102B04	29176	55	42	67
102B04	29177	57		69
102B04	29180	72	59	84
102B04	29189	74	61	86
102B04	29396	76	63	88
102B15	29387	90	78	101
102B15	29388	92	80	103
102B15	29389	94	82	105
102B15	29390	107	96	109
102B15	29395	108	99	110

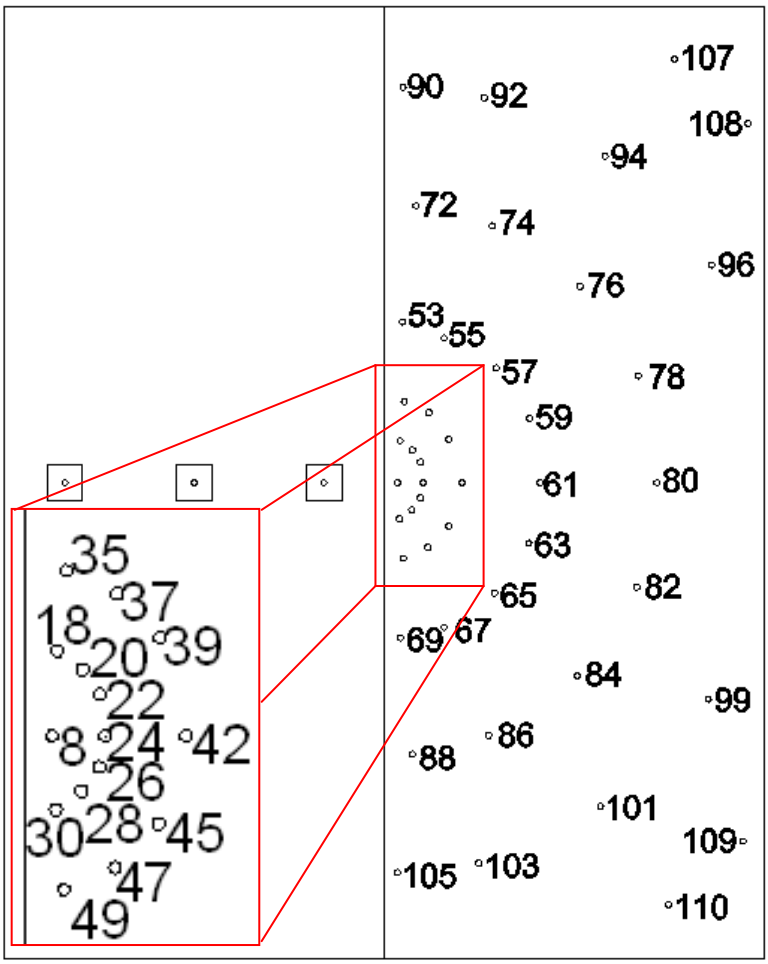

Figure 3.9. Sample point locations and labels.

3.2.3. Data Acquisition System. The Synergy Data Acquisition System was positioned under the transducer-side of the table behind a shield to minimize damage to the computer while maintaining proximity to the transducers and thus eliminating the need for an external signal amplifier. Table 3.3 summarizes the information provided by PCB for each transducer, and used to calibrate the Synergy DAS. In addition to this information, the DAS was set to capture the signal from each transducer as IEPE. The Synergy DAS was set to recorder mode with a decimal timebase and sample rate of 5 µs (200 kS/s). Recorder mode allows the oscilloscope files to be saved and loaded for review at a later time, and the sample rate of 5 µs minimizes the file size while allowing enough samples to be taken to record the pressure peaks accurately.

Table 3.3. Pressure transducer calibration information.

Model Number	Serial Number	Output Bias Level (VDC)	Voltage Sensitivity (mV/psi)	Range (psi)
102B	29322	10.2	1.010	495
102B	29323	10.2	1.009	496
102B	29324	10.2	1.009	496
102B	29325	10.2	1.018	492
102B	29327	10.3	1.038	482
102B04	29178	10.2	5.032	199
102B04	29176	10.1	4.993	200
102B04	29177	10.1	4.989	200
102B04	29180	10.0	5.038	198
102B04	29189	10.1	5.014	199
102B04	29396	10.2	5.063	198
102B15	29387	9.0	24.88	80.4
102B15	29388	10.1	24.47	81.7
102B15	29389	10.1	25.33	79.0
102B15	29390	10.1	24.71	80.9
102B15	29395	10.0	24.82	80.6

3.3. TESTING PROCEDURE

Once the pressure transducers were in place and connected to the Synergry DAS, testing was conducted according to the following procedure:

All cracks or gaps on the table were sealed with duct tape, the table was swept of debris, and the gap between the two sides of the table was eliminated by clamping the sides of the table together to minimize obstacles in the path of the blast wave and to ensure repeatability. Then, C-4 was weighed into 73 (+/- 0.5) gram charges. Each charge was pressed in a hollow, rubber mold to shape it into a hemisphere and then set on the center of a cardboard square which had a ¼" hole drilled through its center. A Dyno Nobel #1 MS Series Masterdet electric detonator was placed through the hole in the cardboard and halfway into the 73 gram hemisphere of C-4. The mold kept the charge from deforming while the detonator was inserted before the mold was removed. After clearing the range of non-essential personnel, the charge assembly was placed on one of the three charge locations, and the Synergy DAS was set to record the pressures from the shot. The detonator lead-in lines were strung and connected to the blast cable, which was shunted on the firing end. Finally, the blast cable was connected to an electric blasting machine. The range was checked once more to ensure it was clear, and the charge was detonated. The Synergy DAS was stopped, and the data was saved for later review.
To ensure the quality control of the experiments, each procedure was repeated according to the above description. Because any variation in the setup could significantly affect the results, the charges were placed in the same location at each standoff position and the detonators were inserted the same depth in the charge for every shot. To remove any potential disturbance from the table, all of the debris was cleared prior to each shot. The

wall height and pressure transducer array were not changed until each test requiring that specific height and array was completed so there was no configuration difference in tests of the same wall height or array. The test matrix (Table 3.4) shows that the tests for all three standoffs were repeated for the first wall height and array. Then the array was moved, keeping the wall height the same, and the nine tests for the three standoff distances were completed again. This was repeated once more until all arrays and standoff distances were tested for the first wall height. After the first 27 tests were completed, the wall height was changed and the next set of 27 tests were completed. Finally, the wall was set at its final height and the final 27 tests were conducted. All three tests of each variable combination were completed on the same day to eliminate weather as a factor in the results. In addition, all test sets were completed on days with similar weather (partly cloudy, approximately 70°F, and little to no wind) at the elevation of approximately 1150 ft above sea level. The Blast Effects Computer was used to determine the actual effect that elevation and temperature has on the pressures created by an explosive charge. An elevation change of 1,750 ft is required to change the pressure of a blast by one psi. Also, temperature has an effect on the arrival time of the pressure and not on the magnitude of the pressure. A change of 50° F is required to change the arrival time by 1 ms (Blast Effects Computer, 2001). After this analysis, it is obvious that the chance that weather has any effect on the results is relatively low compared to the other factors mentioned throughout the report that may have caused variability in the results. These other factors include the depth of placement of the detonator in the charge because this could have caused variability in the data.

Table 3.4. Test matrix.

Test Number	Standoff (mm)	Array	Wall Height (mm)
1, 2, 3	387	1	0
4, 5, 6	1219	1	0
7, 8, 9	2046	1	0
10, 11, 12	387	2	0
13, 14, 15	1219	2	0
16, 17, 18	2046	2	0
19, 20, 21	387	3	0
22, 23, 24	1219	3	0
25, 26, 27	2046	3	0
28, 29, 30	387	1	73
31, 32, 33	1219	1	73
34, 35, 36	2046	1	73
37, 38, 39	387	2	73
40, 41, 42	1219	2	73
43, 44, 45	2046	2	73
46, 47, 48	387	3	73
49, 50, 51	1219	3	73
52, 53, 54	2046	3	73
55, 56, 57	387	1	226
58, 59, 60	1219	1	226
61, 62, 63	2046	1	226
64, 65, 66	387	2	226
67, 68, 69	1219	2	226
70, 71, 72	2046	2	226
73, 74, 75	387	3	226
76, 77, 78	1219	3	226
79, 80, 81	2046	3	226

3.4. DATA RECOVERY AND MANIPULATION

Once testing was completed, each pressure recording (Figure 3.10) was individually analyzed and the peak pressures recorded for each sample location. Figure 4.1 illustrates an example of one of the tests' multiple pressure recordings (shot 6: 1219

mm standoff, 0 mm wall height, array 1) and shows the pressure wave for each of the 16 sample locations and the relative timing of the arrivals.

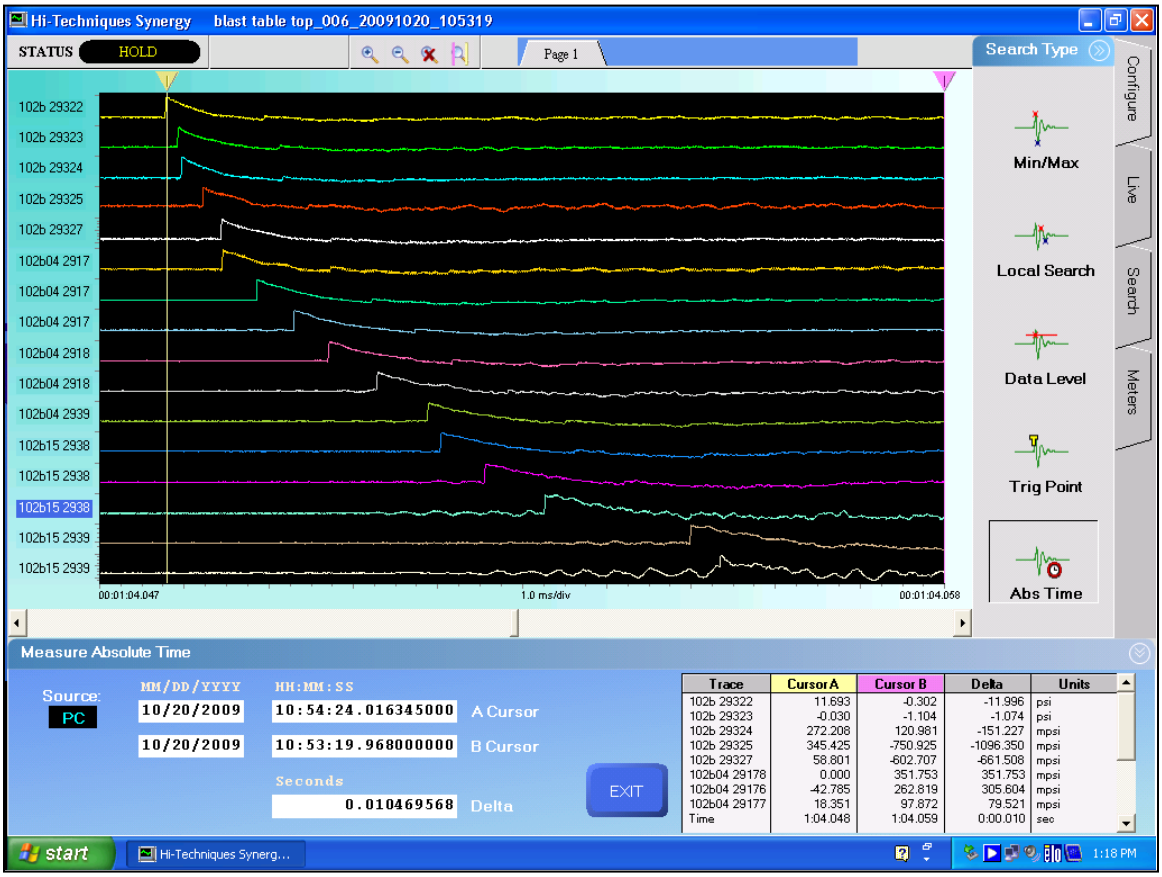

Figure 3.10. Screenshot of a free-field, 1219 mm standoff test data set.

For each combination of wall height, standoff distance, and transducer array, three tests were completed for repeatability. Thus, there were 27 setup combinations and 81 tests. The results from each of the three tests of same wall height, standoff distance, and transducer array were averaged at each individual data point location on the table to create a “pressure set,” at each pressure recording point. The average of the three

pressures from each sample point was used to more accurately represent the performance of the wall. The averaged results were recorded with the location of the data point and the combination of variables used (Table 3.5 and Appendix). The data recorded from the comparison test between the steel plate and cardboard plate gave a 15% difference between the steel and the cardboard. Because of this, the data recorded when using the cardboard plate had to be increased by 15% to account for the difference, as shown in the Adjusted Pressure column in Table 3.5 and Appendix. Finally, the coordinate system for the sample points sets the y-coordinate as the location along the length of the wall and the x-coordinate as the distance away from the wall. The origin of the system is at the center point of the wall and the axis running through the charge locations.

Table 3.5. Example of test results (387 mm standoff distance).

Point	Y-Coordinates (mm)	X-Coordinates (mm)	Scaled Distance (m/(kg^(1/3)))	0 mm Wall Height, 387 mm Standoff Distance Pressure (Pa)	73 mm Wall Height, 387 mm Standoff Distance Pressure (Pa)	226 mm Wall Height, 387 mm Standoff Distance Pressure (Pa)
8	0.0	84.1	2.42	726,508	55,158	26,216
18	230.2	96.8	7.19	580,612	124,106	25,138
20	174.6	177.8	7.17	475,948	137,895	29,195
22	96.8	231.8	7.23	454,190	151,685	30,654
24	0.0	249.2	7.18	394,199	165,474	32,392
26	-96.8	231.8	7.23	362,042	179,264	34,343
28	-174.6	177.8	7.17	497,043	193,053	32,396
30	-230.2	96.8	7.19	589,702	206,843	26,101
35	484.2	120.7	14.37	327,329	241,317	27,354
37	415.9	279.4	14.42	236,644	255,106	29,581
39	277.8	414.3	14.36	215,208	268,896	29,326
42	0.0	498.5	14.35	190,702	289,580	29,105
45	-277.8	414.3	14.36	219,377	310,264	30,585
47	-415.9	279.4	14.42	253,833	324,054	30,410
49	-484.2	120.7	14.37	353,455	337,843	26,384
53	992.2	103.2	28.72	129,569	365,422	24,099
55	927.1	382.6	28.87	104,945	379,212	28,712
57	708.0	706.4	28.79	86,529	393,001	24,532
59	385.8	925.5	28.87	78,812	406,791	22,806
61	0.0	1000.1	28.79	91,179	420,580	26,228
63	-385.8	925.5	28.87	82,466	434,370	23,300
65	-708.0	706.4	28.79	84,118	448,159	25,478
67	-927.1	382.6	28.87	103,950	461,949	27,593
69	-992.2	103.2	28.72	128,185	475,738	24,679
72	1741.5	181.0	50.41	47,988	496,423	21,454
74	1619.3	671.5	50.47	48,204	510,212	22,256
76	1238.3	1238.3	50.41	41,366	524,002	18,050
78	669.9	1617.7	50.41	38,254	537,791	15,674
80	0.0	1751.0	50.41	37,861	551,581	16,239
82	-669.9	1617.7	50.41	44,844	565,370	16,364
84	-1238.3	1238.3	50.41	39,886	579,160	19,043
86	-1619.3	671.5	50.47	50,162	592,949	20,939
88	-1741.5	181.0	50.41	48,971	606,739	20,445
90	2498.7	84.1	71.98	28,501	620,528	16,603
92	2438.4	606.4	72.34	26,002	634,318	18,156
94	2076.5	1387.5	71.90	25,221	648,107	14,764
96	1387.5	2079.6	71.97	26,402	661,897	13,266
99	-1387.5	2079.6	71.97	30,576	682,581	16,141
101	-2076.5	1387.5	71.90	26,464	696,371	14,851
103	-2438.4	606.4	72.34	26,972	710,160	17,874
105	-2498.7	84.1	71.98	32,412	723,950	18,352
107	2703.5	1822.5	93.86	18,648	737,739	12,392
108	2298.7	2300.3	93.62	21,725	744,634	15,516
109	-2298.7	2300.3	93.62	16,508	751,529	10,802
110	-2703.5	1822.5	93.86	18,034	758,424	12,139

4. RESULTS

Multiple methods were used to study the blast pressures. First, pressure was plotted against scaled distance at angles from the axis. Second, the percent reduction (if any) of the blast pressure behind the barrier wall was plotted. Third, a geometrical relationship between the wall height, standoff distance, and pressure reduction area was examined, and a sensitivity analysis was conducted based on the contour charts and geometric relationship study. Then, the benefits of a blast barrier wall with respect to human tissue damage were examined. Finally, the data were compared to the findings of the USACE (Rickman and Murrell, 2004) to calibrate the data collected at the Missouri S&T test site in Rolla, Missouri, with that collected at the ACE test site in Vicksburg, Mississippi.

The pressure plotted against scaled distance permits comparison among charges of similar geometry and composition detonated in the same atmosphere at the same scaled distance to determine the effect of charge size (Smith and Hetherington, 1994).

The Hopkinson-Cranz scaling law, a widely used approach to scaling, uses cubed-root scaling:

$$Z = R/W^{1/3} \tag{1}$$

The scaled distance (Z) used in this project is calculated in $ft/lb^{1/3}$ by dividing the distance from the blast wall (R) in feet by the third root of the weight of the explosive (W) in pounds.

The charts of pressure versus scaled distance compare the results of the three standoff locations at similar wall heights. These charts give an idea as to how the pressure reduction area changes with regard to the change of location of the charge and the wall height.

The second method of analysis was to create a contour chart of the percent reduction of pressures due to the barrier wall at each wall height and standoff distance. Isolines depicting a given percent reduction from the free-field pressures to the pressures behind the barrier wall at similar charge positions were used to determine the effect of the barrier wall. The locations of the contour lines between the sample points on the table were calculated through linear interpolation using MATLAB, a mathematical programming software package. Linear interpolation stays true to the data points and gives a good visual of the effects of the wall height or standoff distance. Plotting the contours revealed a relatively large amount of pressure reduction close to the wall. The area of pressure reduction is referred to here as the *shadow area* (Figure 4.1).

The inner shadow area is defined as the area of the table affected by the wall at a percent reflected pressure reduction greater than 30%. The outer shadow area is the area affected by the wall at a percent reflected pressure reduction less than 30%, down to zero reflected pressure reduction. The remainder of the area, or the normal area, was not affected by the barrier wall and has similar pressures to the free-field tests. The percent reduction that defines the boundary between the inner and outer shadow areas is fixed at 30% because it gives an ideal depiction of where the wall offers the most protection and where it offers only a minimal amount of protection. There was also a natural break in

the data at approximately that mark. This break is described in greater detail in the next section.

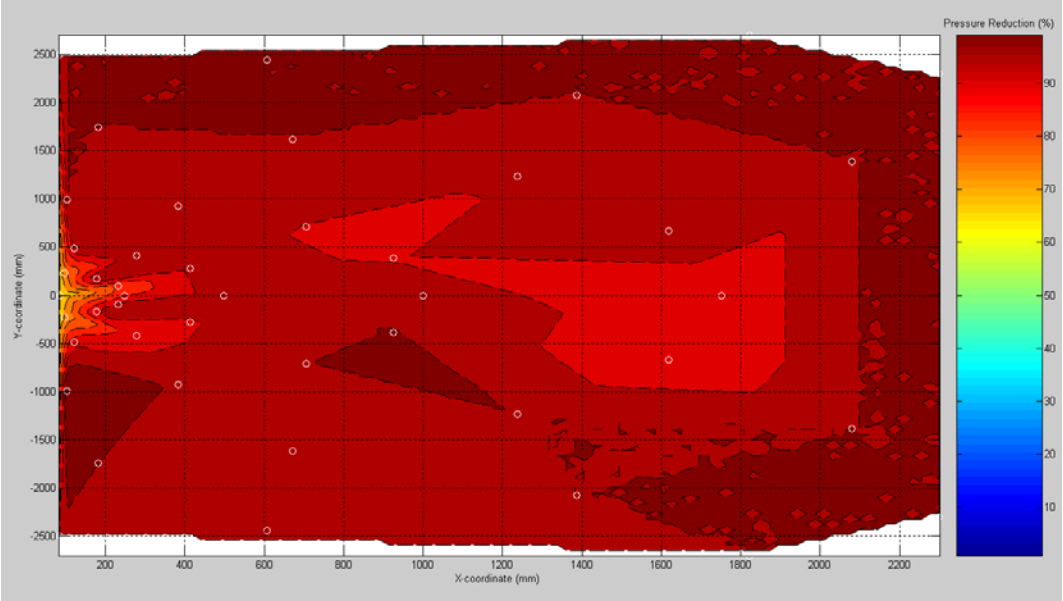

Figure 4.1. Example of shadow area (387 mm standoff, 73 mm wall height).

Further analysis using the percent reduction and contour charts included an examination of the relationship between the geometry of the wall height, standoff distance, and location of the shadow area boundary. This study addressed the relationship shown in Figure 4.2. Logic would indicate that there should be a mathematical model to predict β, and therefore the distance to β, given α by the standoff distance to the charge and the wall height. This hypothesis is examined in Section 5.

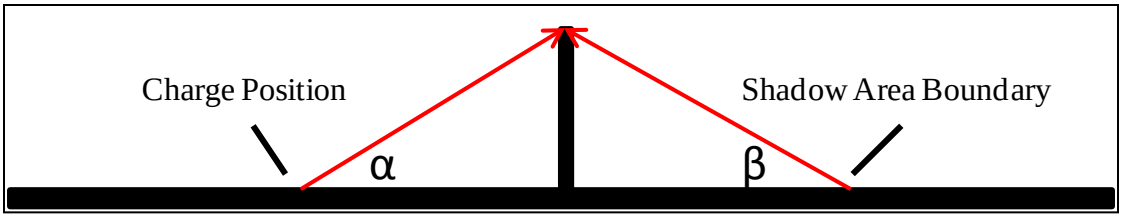

Figure 4.2. Geometric relationship between the wall height, standoff distance, and location of the pressure reduction boundary.

With an understanding of the effects of the barrier wall at the chosen heights, the "health benefits" of a barrier wall is one further area of study. Blast pressures can have a devastating effect on the tissues of the human body, and understanding the percent reduction of the blast pressures can help in appreciating the extent to which a barrier wall can help avert blast damage to a human that may otherwise be severely injured or killed (Zipf and Cashdollar, 2007).

In the calibration test, data from this experiment were graphed with data from experiments 1 and 2 of the USACE report (Rickman and Murrell, 2004). The data from the USACE report are results of a free-field, 30 mm standoff, 72.8 gram charge test (Experiment 1) and a free-field, 90 mm standoff, 72.8 gram charge test (Experiment 2). This project tested the five experiment setup configurations shown in Table 4.1.

Test parameters of the two projects were not identical; therefore those used here were chosen because each has the same explosive charge weight and no interference from a barrier wall. Only the data recorded from sample points on the axis were used. The only difference among the tests was the distances between charge locations and sample points, allowing the data to be graphed on a single chart relating pressure to distance from the explosive charge.

Table 4.1. Free-field tests from Missouri S&T used in comparison with USACE tests.

Tests	ACE	ACE	Missouri S&T	Missouri S&T	Missouri S&T
Wall Height (mm)	0	0	0	0	0
Standoff Distance (mm)	30	90	387	1219	2046
Charge Mass (g)	73	73	73	73	73

5. DISCUSSION

5.1. STATISTICAL ANALYSIS

Statistical analysis of the data shows that the average pressure sets accurately represent the pressures produced by a 73 gram charge with various combinations of wall height and standoff distance. On average, the standard deviation indicates that 95% of the time, the pressure fell within approximately 4% of the mean. For this project, a range of 5% was deemed acceptable; therefore, the data were satisfactory in that respect. A regression analysis of the data on the axis of the table showed that the scatter increases with wall height. The R^2 value is near 1 for the data produced with no barrier wall which means the data had very little scatter. As the wall height increased, the R^2 value dropped to near 0.8, which means the data became scattered as the barrier wall increased in height. The data had no scatter without a barrier wall providing interference because of the free field. With increased interference from the barrier wall, the data became more scattered because of the obstacle.

The error of the pressure transducers is minimal. It is estimated to be less than 0.001%. The percent error was found by estimating the slope of the peak of the tail of each pressure waveform. It was assumed that the slope at that point is linear. The maximum peak pressure that could occur in the 5 μs span between the sample points could be estimated with the slope and the max recorded pressure. The percent different of the estimated and measured peak pressure was less than 0.001%; therefore, the assumption was made that each transducer produced readings with less than 0.001% error.

5.2. PRESSURE VERSUS SCALED DISTANCE

The charts of pressure versus scaled distance were used to plot the results recorded on the axis line of the table in three charts, one for each wall height (Figure 5.1). In this way, the charts illustrate that the barrier wall has a significant effect on the blast pressures, especially at locations close to the wall (those within the shadow area). The charts show a qualitative depiction of the shadow area, and that the shadow area does not drastically change with respect to a change in the standoff distance. In Figure 5.1(a), the chart for a wall height of 0 mm demonstrates the behavior of the blast pressures without a barrier wall. The charts for wall heights of 73 mm and 226 mm (Figures 5.1(b) and

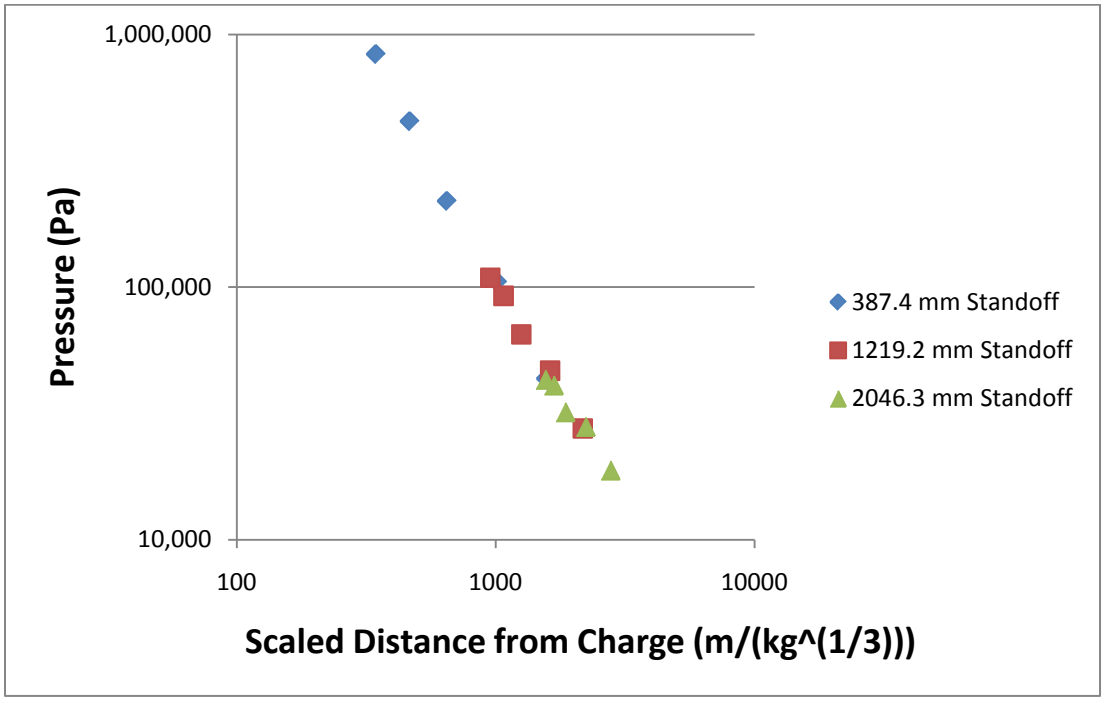

(a) 0 mm wall height.

Figure 5.1. Combined standoff distance tests at wall heights of (a) 0 mm, (b) 73 mm, and (c) 226 mm.

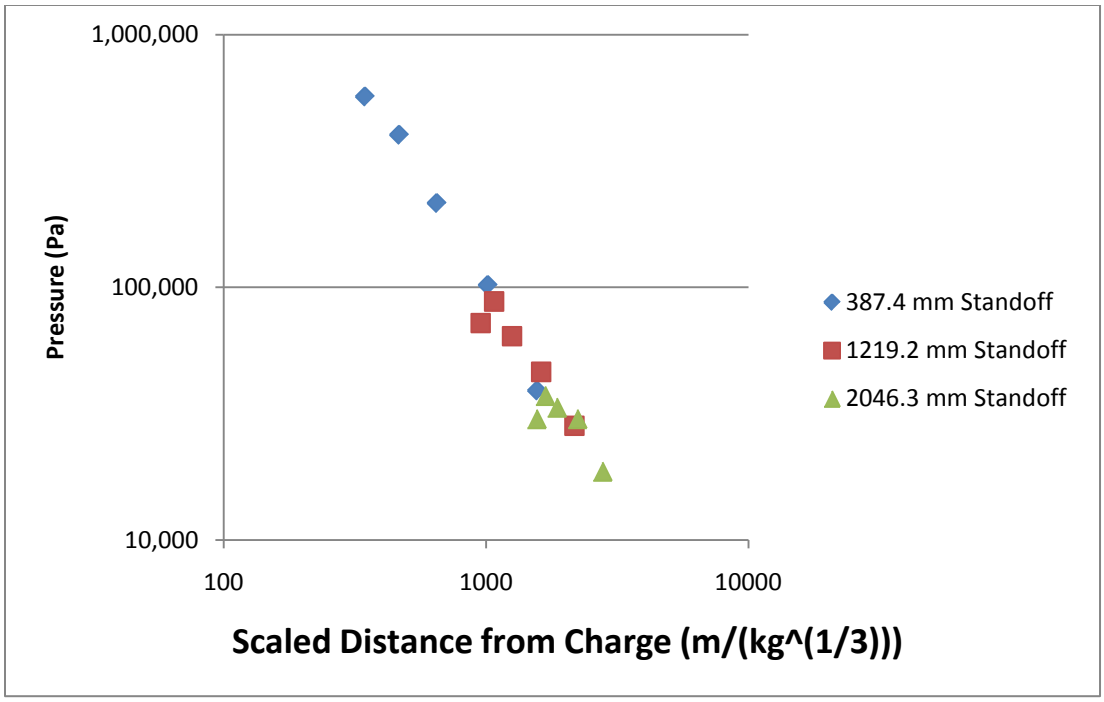

(b) 73 mm wall height.

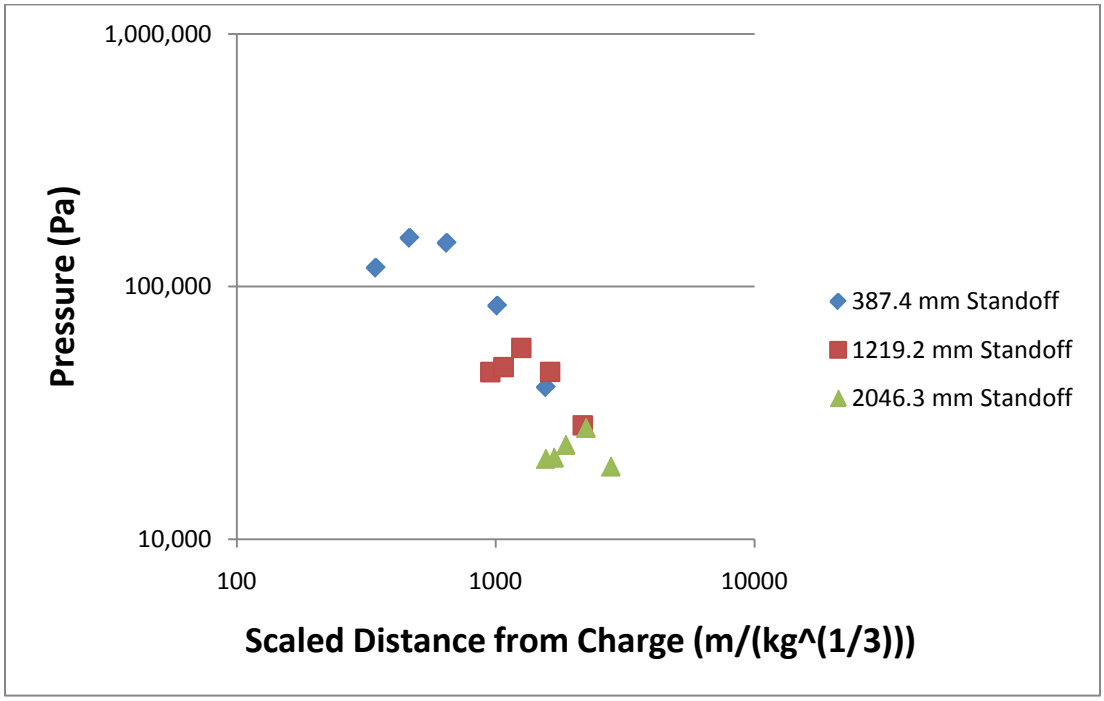

(c) 226 mm wall height.

Figure 5.1. Combined standoff distance tests at wall heights of (a) 0 mm, (b) 73 mm, and (c) 226 mm. (cont.)

5.1(c)) illustrate that an increase in wall height expanded the shadow area. The shadow area changes drastically when the wall height changes; however, when the standoff distance changes, the boundary changes much less noticeably. How the shadow area is affected by the wall height and standoff distance is discussed next.

5.3. CONTOUR ANALYSIS

The contour charts (Figure 5.2) depict the percent reduction from the free-field test pressures to the barrier wall test pressures at similar standoff distances. The colors that range from blue to yellow (inner shadow area) depict a pressure reduction of greater than 30%, and the orange color (outer shadow area) represents a pressure reduction between 0% and 30%. The dark red area shows no pressure reduction between the free field tests and the barrier tests. Visually, the charts exhibit quality data. The 30% pressure reduction boundary was chosen for two reasons. The data displayed a natural break in that area, and the reduction area between 30% and 0% fanned out to cover a larger area than the area with percent reduction greater than 30%, where the data showed a more compact pressure reduction area.

The inner shadow area of the 73 mm barrier wall tests (Figures 5.2(a), 5.2(b), and 5.2(c)) does not show a significant change in size except for where it expands along the length of the wall as the standoff increases; however, the outer shadow area does increase.

A significant change in the shadow area is due to a change in the wall height. The percent change in wall height has a greater impact on the size of the shadow area than the percent change in standoff distance (Figures 5.2(d), 5.2(e), and 5.2(f)). When combining

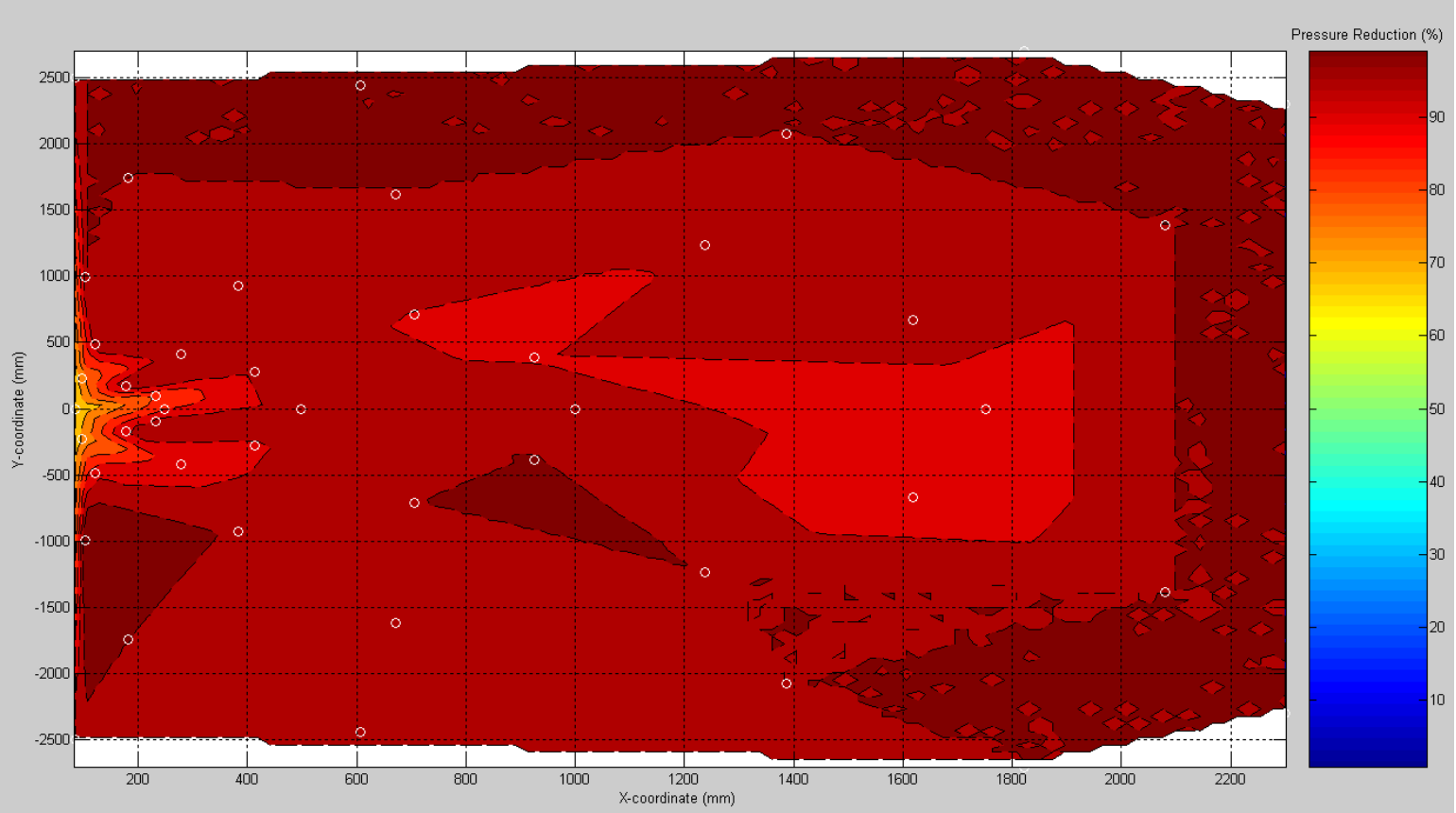

(a) 73 mm wall height, 387 mm standoff.

Figure 5.2. Percent reduction contour charts.

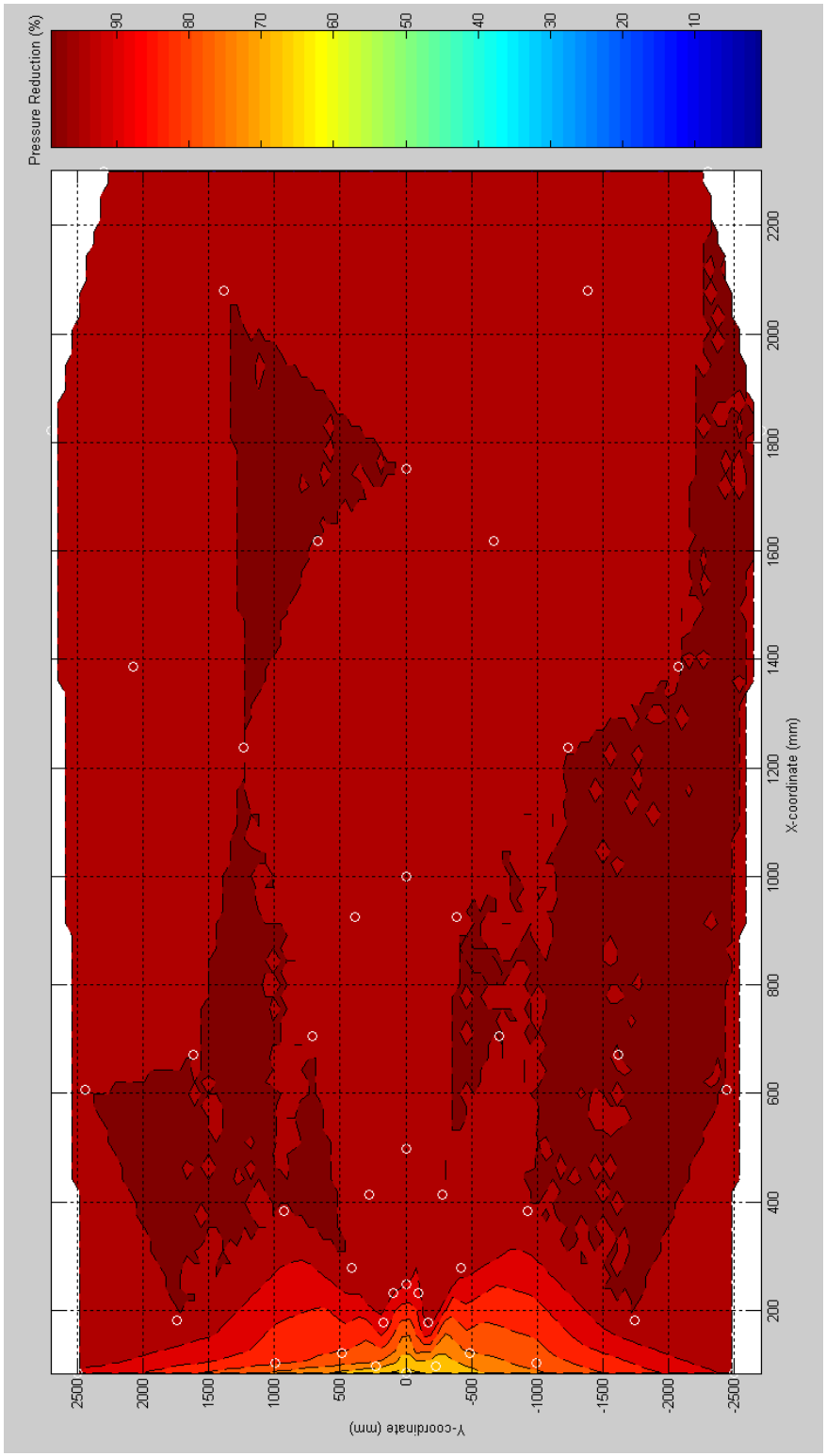

(b) 73 mm wall height, 1219 mm standoff.
Figure 5.2. Percent reduction contour charts. (cont.)

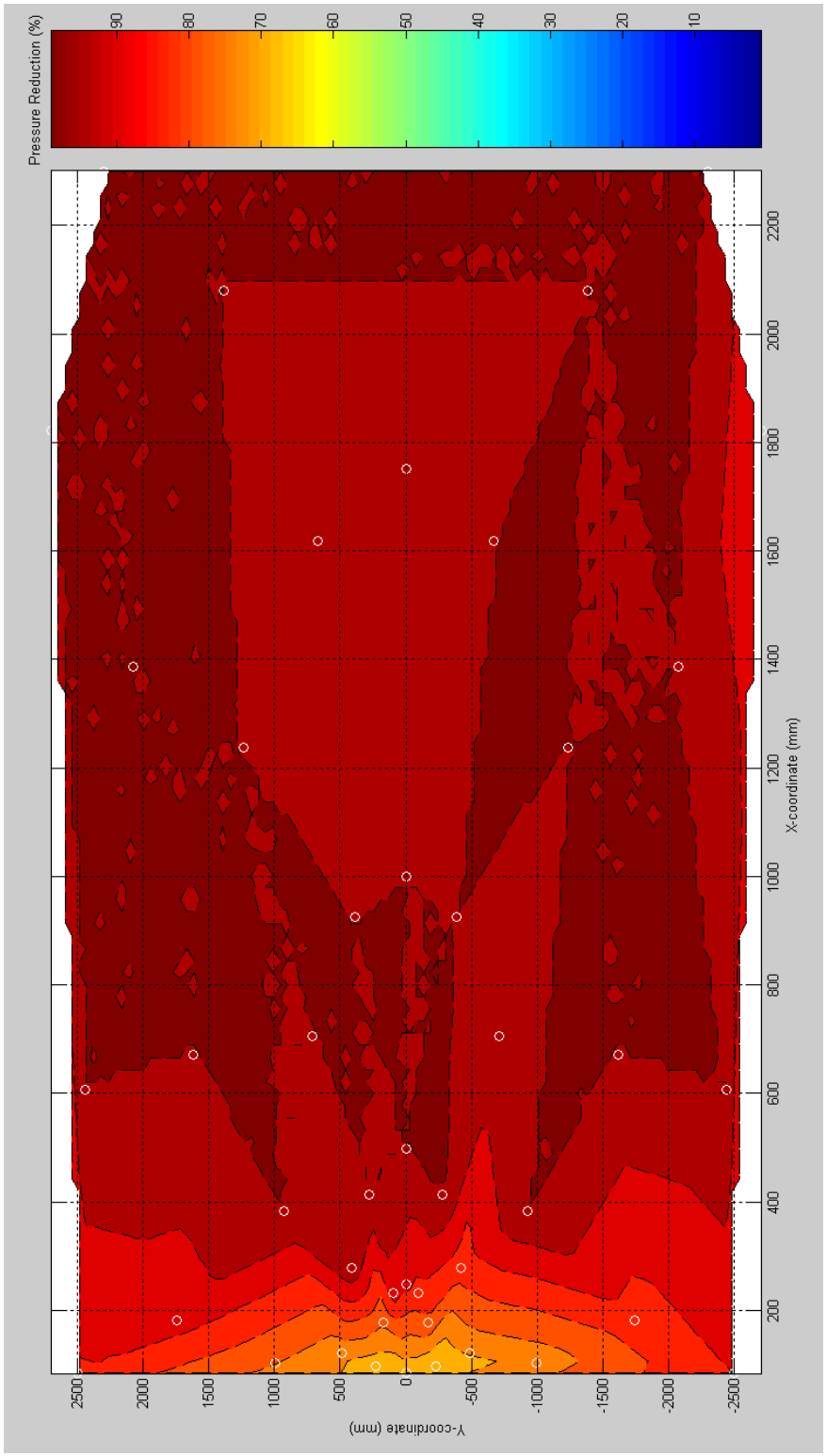

(c) 73 mm wall height, 2046 mm standoff.
Figure 5.2. Percent reduction contour charts. (cont.)

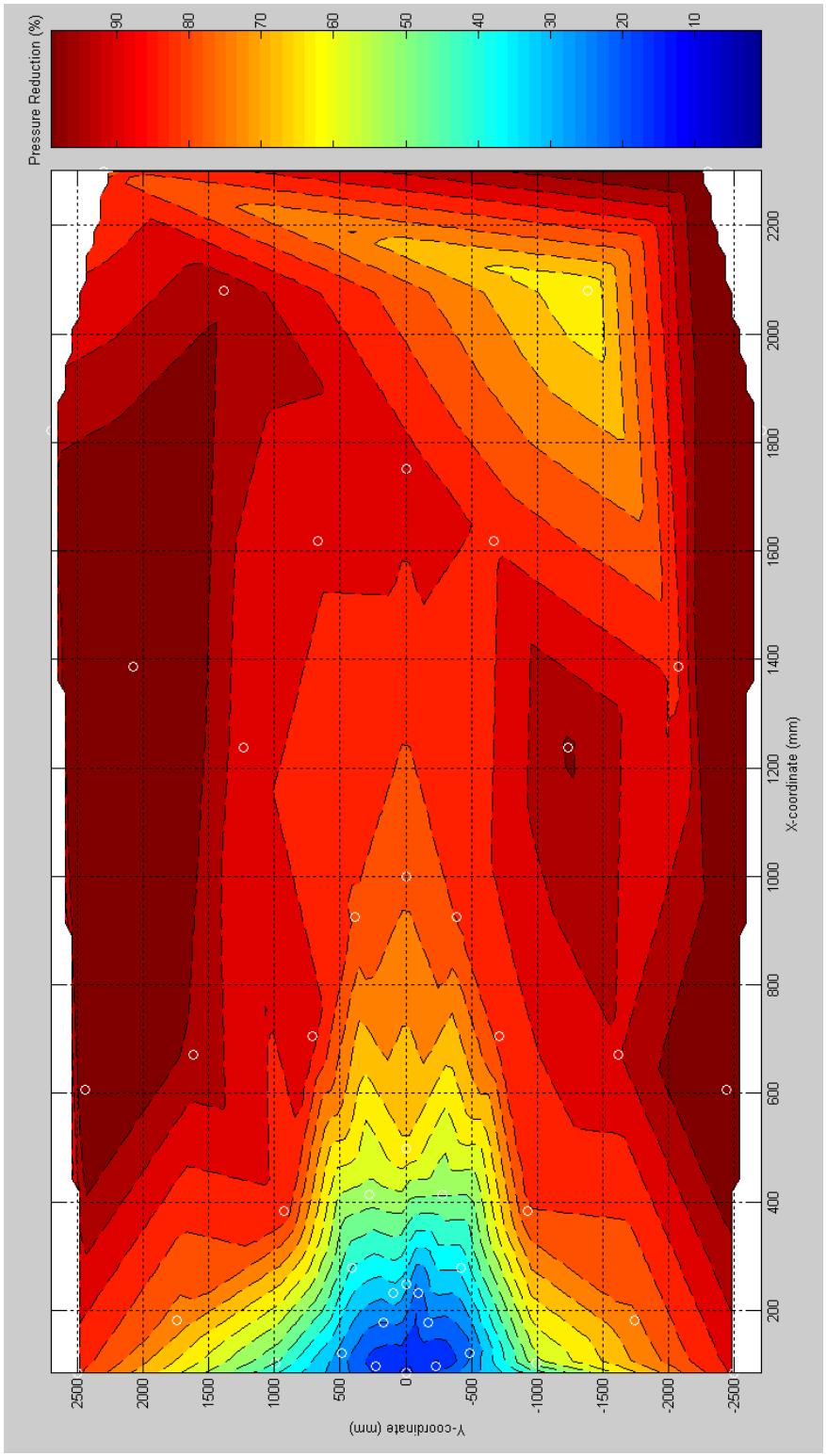

(d) 226 mm wall height, 387 mm standoff.

Figure 5.2. Percent reduction contour charts. (cont.)

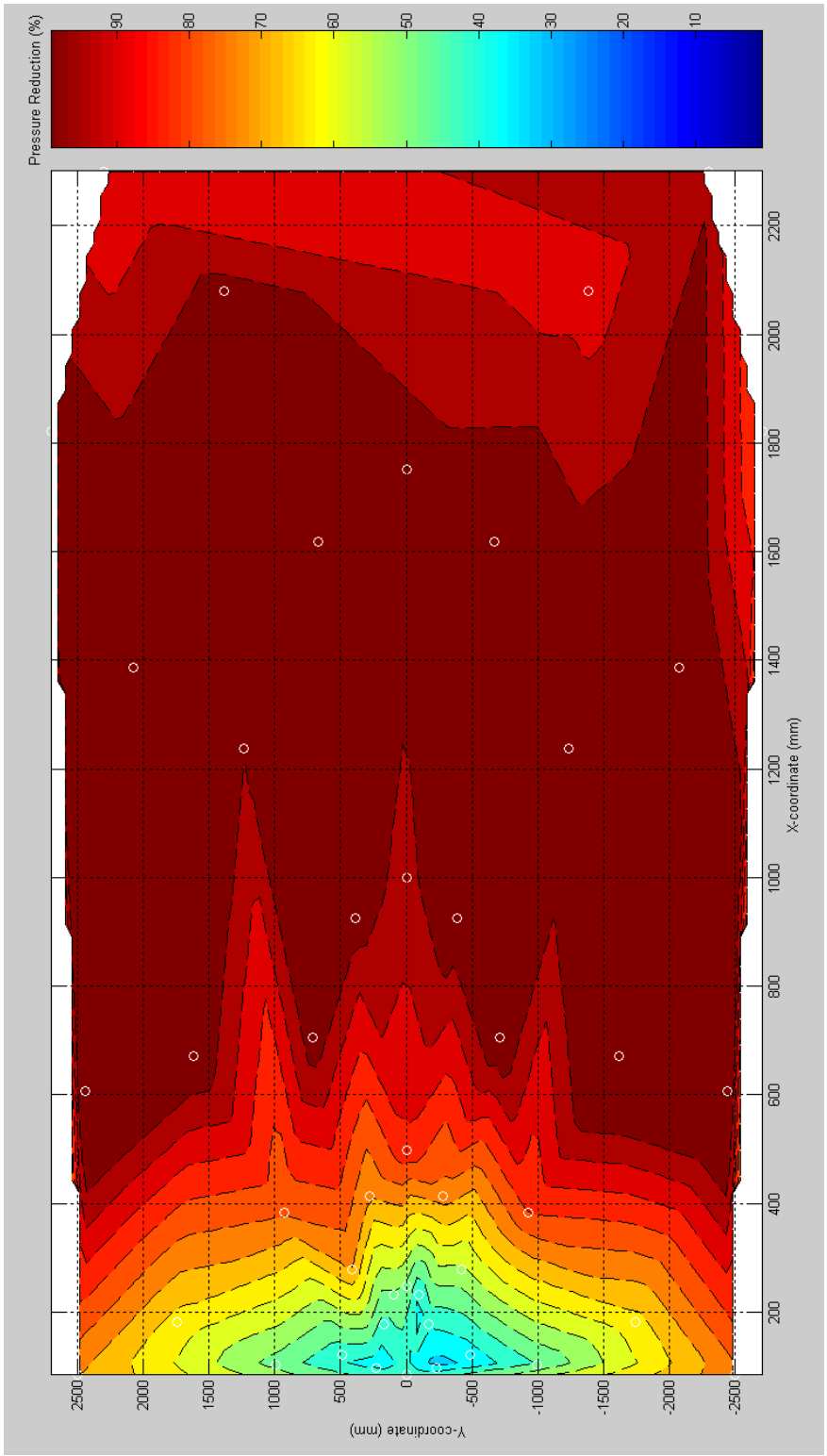

(e) 226 mm wall height, 1219 mm standoff.

Figure 5.2. Percent reduction contour charts. (cont.)

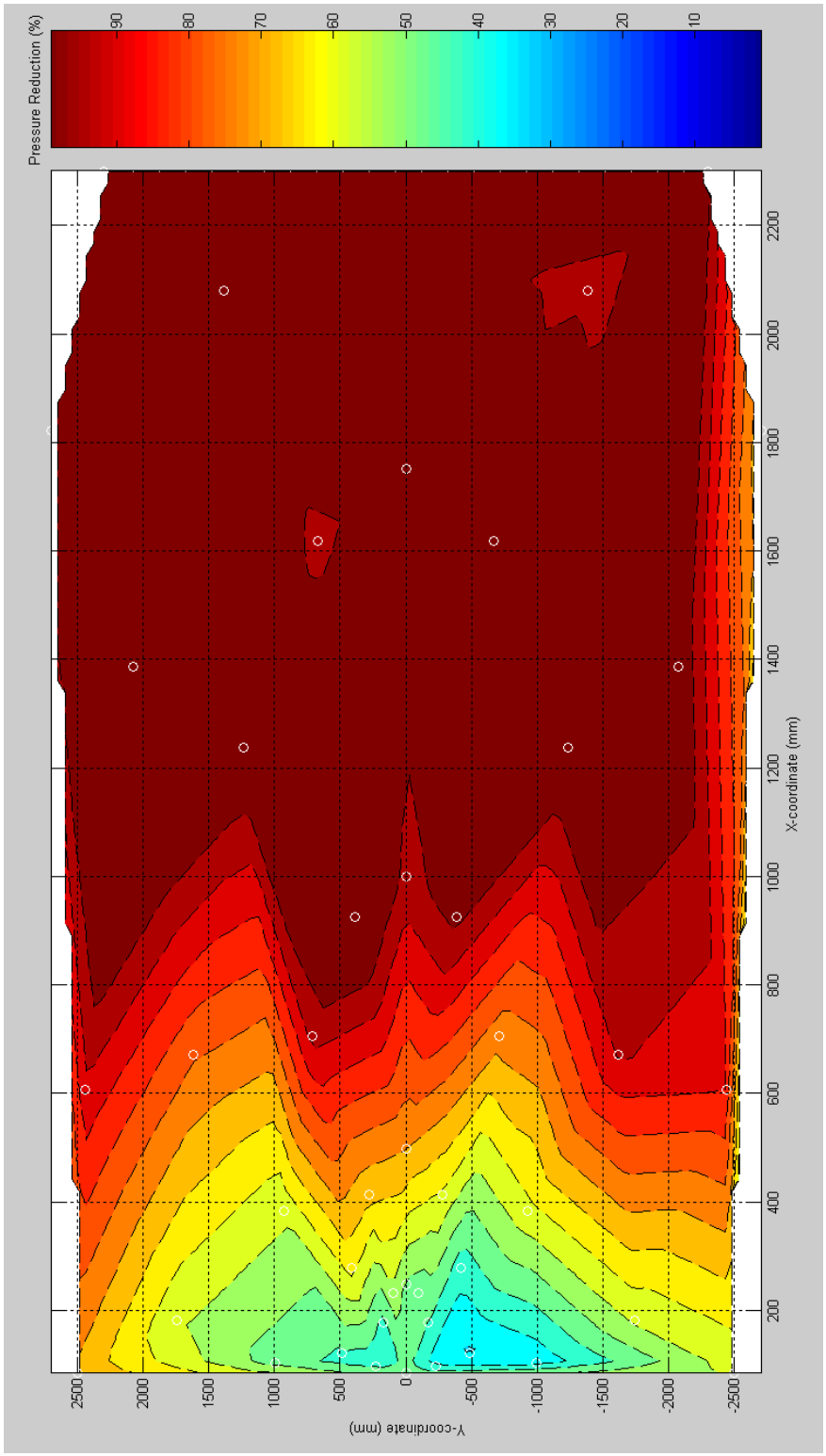

(f) 226 mm wall height, 2046 mm standoff.

Figure 5.2. Percent reduction contour charts. (cont.)

these two observations, it appears that the effect of the barrier wall is enhanced when the standoff distance and wall height increase and vice versa.

If one must be chosen over the other to induce the lowest pressures, a larger standoff distance is preferred over a larger wall height. This is due to the laws of sound propagation that state that as distance from a source is doubled, the pressure drops by a factor of ten. However, in close quarters, a barrier wall could induce a significant pressure drop in short range areas and be a significant factor of pressure reduction in those short range areas.

The contour charts also show the effect that the barrier wall has on the different angles off axis. The section of the shadow area on the axis and the angles off the axis adjacent to the wall becomes larger as the barrier height increases. This means that pressures are reduced more along the wall and directly away from the wall than in the in-between areas.

5.4 GEOMETRIC AND SENSITIVITY ANALYSES

It follows from the contour charts that there should be a geometric relationship between the wall height and standoff distance and the extent of the total shadow area. A relationship between the angles α and β at the outer boundary of the shadow area, as described in Section 4.2, is proposed (Figure 5.3). Figure 5.3 displays the relationship of α, the angle whose tangent is the height of the barrier wall divided by the standoff distance, to β, the angle whose tangent is the height of the barrier wall divided by the length of the inner shadow area. Since the wall height has a greater impact on the shadow area than the standoff, separate groupings were graphed for each wall height.

Additionally, the wall heights must be grouped separately because two dissimilar wall heights could have an equivalent β depending on the standoff distance. Each β must be matched with its corresponding wall height to calculate the length of the corresponding shadow area for each separate β. The results can be graphed on the same graph; however, they must be related in groups corresponding to the wall height of each group as stated above (Figure 5.3).

Figure 5.3 also shows the effect of the standoff distance on the shadow area. In addition, the chart shows that the standoff distance has less of an effect on the shadow area as the wall increases in height. Therefore, if the wall has enough height, the length of the standoff distance will have less of an impact on the shadow area than the wall height and β will have little to no change, which means that the shadow area will have little to no change (as in the 226 mm wall height example). In contrast, if the wall height is minimal, then the magnitude of the standoff will have a greater impact, β will have a greater range, and the shadow area will be more susceptible to change. This describes how much more of an effect the wall height has on the percent reduction of the blast pressure than the standoff distance. The graph also shows that as the standoff decreases, α increases. An increase in α equals an increase in β, meaning the extent of the shadow area where blast pressures are reduced decreases.

Logic dictates that the relationship between α and β is linear and geometric; therefore, the graph of any wall height should fall on the same line. Contrary to logic, the data do not fall on the same line; therefore, β is not strictly geometric. The power-law relational differences between the two curves decreases relative to a decrease in the wall

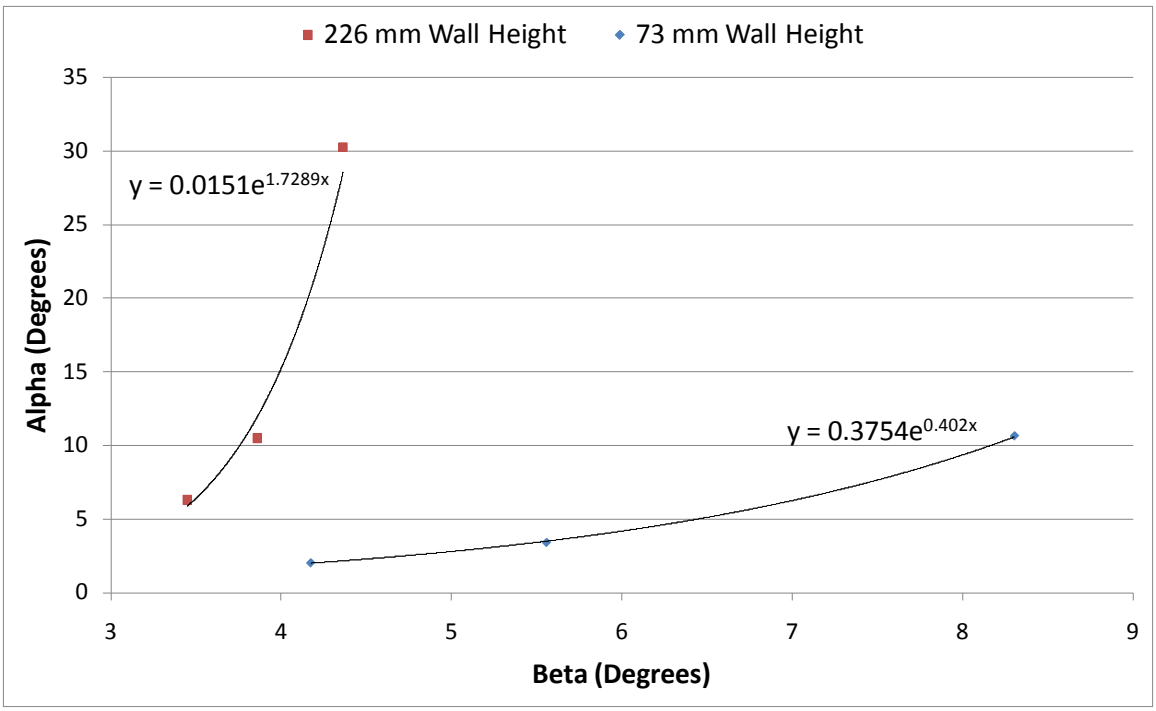

Figure 5.3. Relationship of alpha to beta at the shadow area boundary

height since the impact of the standoff distance on the shadow area increases with a decrease in wall height.

As described above, the wall height and standoff distance both have an impact on the shadow area boundaries. A sensitivity analysis (Figure 5.4) shows just how much of an impact each of these parameters can have. The diagram depicts how much impact a 1% increase in either wall height or standoff distance can have on the shadow area depending on what the other parameter is set at. For instance, a 1% increase in the wall height at the 387 mm standoff distance will increase the shadow area by almost 3%. The analysis shows that the shadow area is approximately ten times more sensitive to a change in the wall height than a change in the standoff distance.

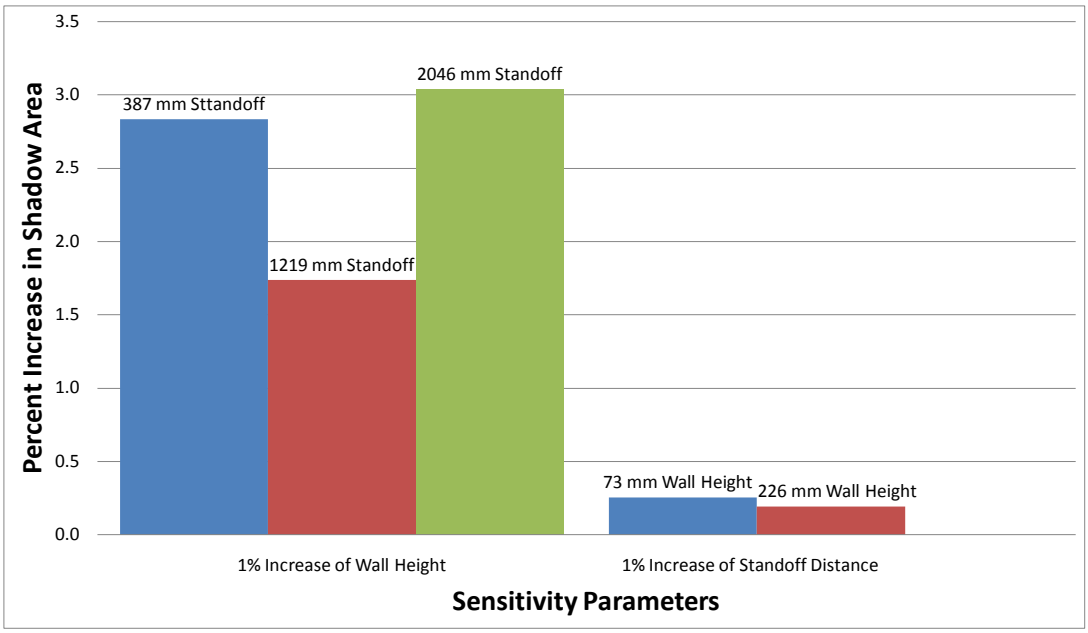

Figure 5.4. Sensitivity analysis of wall height and standoff distance.

5.5. EFFECT ON THE HUMAN BODY

The final study based on the shadow area associates the pressures that cause certain types of human tissue damage and whether or not a barrier wall can reduce the chance of attaining that damage by reducing the associated blast pressures on humans protected by barrier walls (Table 5.1). For this study, assume a direct 1:50 scale-up of the geometry of the blast table tests, charge size, and pressure. When scaling up the size of an explosive charge to gain the equivalent scale-up of pressure, the charge mass is proportional to the cube of the scaling factor (Cooper, 1996). Therefore, a 9,071 kg (20,000 lb) charge produces the same pressures as a 73 gram (0.16 lb) charge at 50 times the distance of the 73 gram charge. For instance, an 9,071 kg charge of C-4 could cause fatalities up to 27.4 m (90 ft) distance (Zipf and Cashdollar, 2007 and Blast Effects Computer, 2001), and if that same charge were placed 19.2 m (63 ft) away from a 3.7 m

Table 5.1. Health Effects (Data from Zipf and Cashdollar, 2007 and Blast Effects Computer, 2001).

Standoff	Height	Fatalities	Lung Damage	Eardrum Rupture
N/A	0 m (0 ft)	27.4 m (90 ft)	>45.7 m (150 ft)	100%
19.2 m (63 ft)	3.7 m (12 ft)	0%	>45.7 m (150 ft)	<100%
19.2 m (63 ft)	11.3 m (37 ft)	0%	0%	<100%
61.0 m (200ft)	0 m (0 ft)	0%	0%	>0%
61.0 m (200 ft)	11.3 m (37 ft)	0%	0%	0%
102.4 m (336 ft)	3.7 m (12 ft)	0%	0%	0%

(12 ft) high barrier wall, as simulated by the 73 mm (2.9 in) high wall tests with a 387 mm (15.2 in) charge standoff distance, the chance of casualties behind that wall would drop to zero and the chance of eardrum rupture would drop below 100% because there would be enough pressure reduction (Zipf and Cashdollar, 2007 and Blast Effects Computer, 2001). However, if the same 9,071 kg charge of C-4 were shot at the same standoff distance from a 11.3 m (37 ft) high barrier wall, as in the 226 mm (8.9 in) high wall tests with a 387 mm standoff, the pressure would drop below the threshold for lung damage, even though lung damage would normally occur over 45.7 m (150 ft) away from the blast with either free-field or a 12 ft high barrier wall present (Zipf and Cashdollar, 2007 and Blast Effects Computer, 2001). Increasing the standoff distance from the wall to 61.0 m (200 ft) (simulated by the 1219 mm (48.0 in) standoff) or 102.4 m (336 ft) (simulated by the 2046 mm standoff) drops all chance of fatalities and lung damage; however, eardrum rupture is still a factor and the reduction of the pressure in the shadow area due to the wall will drop the percent chance of eardrum rupture (Zipf and Cashdollar, 2007 and Blast Effects Computer, 2001). At 61.0 m, an 11.3 m high wall will decrease the chance of eardrum rupture to zero, and at 102.4 m, a wall height of 3.7

m will decrease the chance of eardrum rupture to zero (Zipf and Cashdollar, 2007 and Blast Effects Computer, 2001).

5.6. CALIBRATION ANALYSIS

The final task of this project was to compare the results from the Missouri S&T tests to those from the USACE research. The data from two 73 gram free-field tests conducted by the USACE were first compared to those from the three 73 gram free-field tests conducted at Missouri S&T. The standoff distances for the two projects were different; therefore, the two blast tables were calibrated by plotting pressure versus scaled distance (Figure 5.5). Such a plot is possible because the explosive weight and geometry, wall height, and sample point locations were the same for both projects. The 15% correction factor was included in the Missouri S&T results.

The two free-field tests conducted by the USACE using 73 gram C-4 charges had standoff distances of 30 mm and 90 mm. These were compared to the free-field tests conducted for this project at standoff distances of 387 mm, 1219 mm, and 2046 mm. As can be seen in Figure 5.5, the data from both tests conform to the trendline; therefore, the data from either test do not need calibration to be used in tandem.

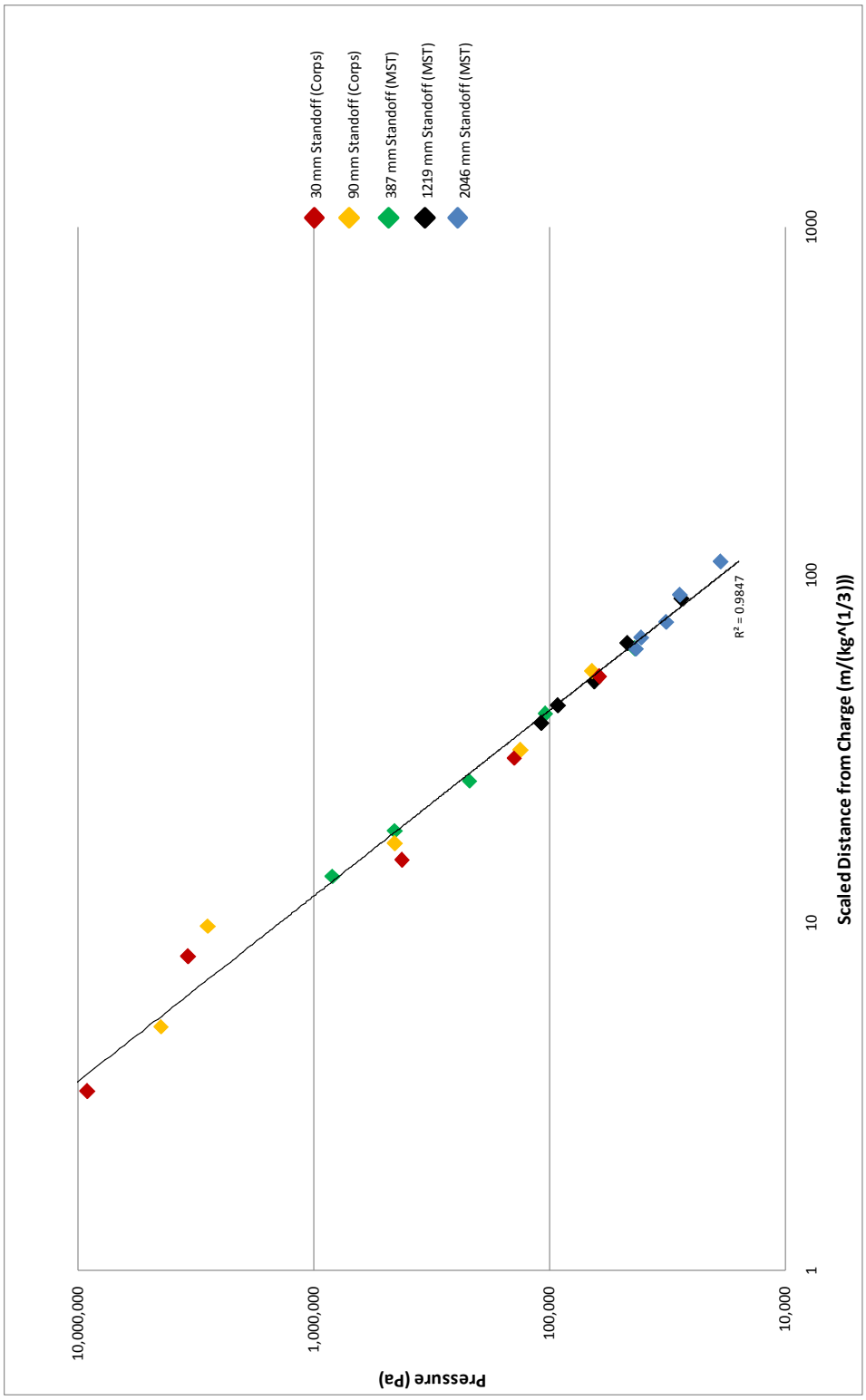

Figure 5.5. Comparison of free-field data from USACE and Missouri S&T tests.

6. CONCLUSIONS AND RECOMMENDATIONS

6.1. CONCLUSION

Because of the testing involved in this thesis, a large amount of data was recorded and used to successfully analyze the effects of a blast barrier wall at three heights.

The charts of pressure versus scaled distance were important to see the shadow area created by the blast barrier wall without the need for any calculations. Once the charts of pressure versus scaled distance gave an illustration of the so-called shadow area, an in-depth analysis using percent reduction of pressure due to the barrier wall was conducted.

The first study was to determine how far the shadow area extended. This gave an idea as to how much the barrier wall influenced the blast pressures. The effect of the wall in the outer shadow area amounted to only a modest reduction of blast pressures, which is contrary to the wall's effect on the inner shadow area. Additionally, the wall has more of an effect on the pressures affecting the area adjacent to the wall than in the open areas away from the wall. The shadow area was greatly influenced by changes in the height of the wall, while changes in the standoff distance of the charge had relatively little influence on the shadow area.

The next step after constructing the contour charts was to determine a geometric relationship between the standoff distance, wall height, and shadow area. The angle equal to the tangent of the wall height and the standoff distance is related to the angle equal to the tangent of the wall height and the boundary of the shadow area, as described in Section 4.2. The exact relationship between the two angles is dependent on the

specific wall height and is not strictly geometric; however, the angles are related and can be graphed to predict the extent of the shadow area given a certain wall height and standoff distance (Figure 5.3).

A sensitivity analysis using the information gained from the contour and geometric studies revealed that a 1% change in wall height had ten times greater effect on the shadow area than a 1% change in standoff distance. It is significant to find that changes in the height of the wall have more of an effect on the shadow area than changes in the standoff distance of the charge. A combination of a large standoff distance and a high wall height is preferable. However, if one must be chosen over the other to induce the lowest pressures; a larger standoff distance is preferred over a larger wall height. Nevertheless, in close quarters, a barrier wall could induce a significant pressure drop in short range areas and would be a sizeable factor of the reduction of the pressures felt in those short range areas.

Finally, barrier walls can have a positive effect on the casualty and injury rates of persons in a position behind a barrier wall. A wall could induce a pressure reduction significant enough to decrease the casualty and injury rates depending on the combination of charge weight, standoff distance, location of the person, and wall height.

This project created a large database and introduced new methods of analysis such as the relationship of α and β for future use by blast barrier researchers and designers. The data gained from this project are not only repeatable, but can be combined with the data gained from the USACE project with no need for calibration. The data can be used to help predict the effects of various wall heights on the blast pressures from a charge at

various standoff distances, and thus to aid in computer modeling, blast barrier prediction, or any other type of research or design that requires empirical data on blast barrier walls.

6.2 FUTURE WORK AND RECOMMENDATIONS

Future work on blast barrier walls should expand the database by testing more wall heights, data points, and standoff distances. The tests completed in this project should be repeated a number of times to increase the number of recorded pressures at each point and develop a more accurate average pressure at each point, permit better statistical analysis of the project, and decrease the confidence interval at each point.

Additional work that could be completed with this experimental setup is a study of the effects of the barrier wall on the blast pressures on the charge side of the wall if sample points could be added to the table. In addition, the thickness of the barrier wall and the impulse of the blast pressure waves are variables that were left open to future research. A relatively thicker wall may aid in the mitigation of the blast wave. Also, the blast impulse (the integral of the pressure versus time curve of the blast data) is another factor that is important in analyzing structural and human tissue damage. Higher impulse increases the susceptibility of structures to blast damage and lowers the threshold at which human tissue can withstand blast pressures.

Finally, if further research is to be done following the procedure used in this project, it is recommended that some details be taken into account. Calibration points outside of the shadow area and at the same location for all tests should be included in

every shot to ensure each shot has equivalent results. Also, symmetry tests could be completed for the two sides of the table to prove the pressures have symmetry and then only one side of the table would need to be tested.

APPENDIX

Point	Y-Coordinates (mm)	X-Coordinates (mm)	Scaled Distance (m/(kg^(1/3)))	0 mm Wall Height, 387 mm Standoff Distance Pressure (Pa)	73 mm Wall Height, 387 mm Standoff Distance Pressure (Pa)	226 mm Wall Height, 387 mm Standoff Distance Pressure (Pa)
8	0.0	84.1	2.42	726,508	55,158	26,216
18	230.2	96.8	7.19	580,612	124,106	25,138
20	174.6	177.8	7.17	475,948	137,895	29,195
22	96.8	231.8	7.23	454,190	151,685	30,654
24	0.0	249.2	7.18	394,199	165,474	32,392
26	-96.8	231.8	7.23	362,042	179,264	34,343
28	-174.6	177.8	7.17	497,043	193,053	32,396
30	-230.2	96.8	7.19	589,702	206,843	26,101
35	484.2	120.7	14.37	327,329	241,317	27,354
37	415.9	279.4	14.42	236,644	255,106	29,581
39	277.8	414.3	14.36	215,208	268,896	29,326
42	0.0	498.5	14.35	190,702	289,580	29,105
45	-277.8	414.3	14.36	219,377	310,264	30,585
47	-415.9	279.4	14.42	253,833	324,054	30,410
49	-484.2	120.7	14.37	353,455	337,843	26,384
53	992.2	103.2	28.72	129,569	365,422	24,099
55	927.1	382.6	28.87	104,945	379,212	28,712
57	708.0	706.4	28.79	86,529	393,001	24,532
59	385.8	925.5	28.87	78,812	406,791	22,806
61	0.0	1000.1	28.79	91,179	420,580	26,228
63	-385.8	925.5	28.87	82,466	434,370	23,300
65	-708.0	706.4	28.79	84,118	448,159	25,478
67	-927.1	382.6	28.87	103,950	461,949	27,593
69	-992.2	103.2	28.72	128,185	475,738	24,679
72	1741.5	181.0	50.41	47,988	496,423	21,454
74	1619.3	671.5	50.47	48,204	510,212	22,256
76	1238.3	1238.3	50.41	41,366	524,002	18,050
78	669.9	1617.7	50.41	38,254	537,791	15,674
80	0.0	1751.0	50.41	37,861	551,581	16,239
82	-669.9	1617.7	50.41	44,844	565,370	16,364
84	-1238.3	1238.3	50.41	39,886	579,160	19,043
86	-1619.3	671.5	50.47	50,162	592,949	20,939
88	-1741.5	181.0	50.41	48,971	606,739	20,445
90	2498.7	84.1	71.98	28,501	620,528	16,603
92	2438.4	606.4	72.34	26,002	634,318	18,156
94	2076.5	1387.5	71.90	25,221	648,107	14,764
96	1387.5	2079.6	71.97	26,402	661,897	13,266
99	-1387.5	2079.6	71.97	30,576	682,581	16,141
101	-2076.5	1387.5	71.90	26,464	696,371	14,851
103	-2438.4	606.4	72.34	26,972	710,160	17,874
105	-2498.7	84.1	71.98	32,412	723,950	18,352
107	2703.5	1822.5	93.86	18,648	737,739	12,392
108	2298.7	2300.3	93.62	21,725	744,634	15,516
109	-2298.7	2300.3	93.62	16,508	751,529	10,802
110	-2703.5	1822.5	93.86	18,034	758,424	12,139

Table A.1. 387 mm standoff distance test data (Metric Units).

Point	Y-Coordinates (in)	X-Coordinates (in)	Scaled Distance (ft/(lb^(1/3)))	0 mm Wall Height, 387 mm Standoff Distance Pressure (psi)	73 mm Wall Height, 387 mm Standoff Distance Pressure (psi)	226 mm Wall Height, 387 mm Standoff Distance Pressure (psi)
8	0.0	3.3	6.09	105.37	8.00	3.80
18	9.1	3.8	18.08	84.21	18.00	3.65
20	6.9	7.0	18.04	69.03	20.00	4.23
22	3.8	9.1	18.18	65.87	22.00	4.45
24	0.0	9.8	18.04	57.17	24.00	4.70
26	-3.8	9.1	18.18	52.51	26.00	4.98
28	-6.9	7.0	18.04	72.09	28.00	4.70
30	-9.1	3.8	18.08	85.53	30.00	3.79
35	19.1	4.8	36.12	47.48	35.00	3.97
37	16.4	11.0	36.27	34.32	37.00	4.29
39	10.9	16.3	36.11	31.21	39.00	4.25
42	0.0	19.6	36.08	27.66	42.00	4.22
45	-10.9	16.3	36.11	31.82	45.00	4.44
47	-16.4	11.0	36.27	36.82	47.00	4.41
49	-19.1	4.8	36.12	51.26	49.00	3.83
53	39.1	4.1	72.20	18.79	53.00	3.50
55	36.5	15.1	72.59	15.22	55.00	4.16
57	27.9	27.8	72.39	12.55	57.00	3.56
59	15.2	36.4	72.57	11.43	59.00	3.31
61	0.0	39.4	72.39	13.22	61.00	3.80
63	-15.2	36.4	72.57	11.96	63.00	3.38
65	-27.9	27.8	72.39	12.20	65.00	3.70
67	-36.5	15.1	72.59	15.08	67.00	4.00
69	-39.1	4.1	72.20	18.59	69.00	3.58
72	68.6	7.1	126.73	6.96	72.00	3.11
74	63.8	26.4	126.88	6.99	74.00	3.23
76	48.8	48.8	126.75	6.00	76.00	2.62
78	26.4	63.7	126.73	5.55	78.00	2.27
80	0.0	68.9	126.74	5.49	80.00	2.36
82	-26.4	63.7	126.73	6.50	82.00	2.37
84	-48.8	48.8	126.75	5.79	84.00	2.76
86	-63.8	26.4	126.88	7.28	86.00	3.04
88	-68.6	7.1	126.73	7.10	88.00	2.97
90	98.4	3.3	180.96	4.13	90.00	2.41
92	96.0	23.9	181.87	3.77	92.00	2.63
94	81.8	54.6	180.76	3.66	94.00	2.14
96	54.6	81.9	180.95	3.83	96.00	1.92
99	-54.6	81.9	180.95	4.43	99.00	2.34
101	-81.8	54.6	180.76	3.84	101.00	2.15
103	-96.0	23.9	181.87	3.91	103.00	2.59
105	-98.4	3.3	180.96	4.70	105.00	2.66
107	106.4	71.8	235.99	2.70	107.00	1.80
108	90.5	90.6	235.38	3.15	108.00	2.25
109	-90.5	90.6	235.38	2.39	109.00	1.57
110	-106.4	71.8	235.99	2.62	110.00	1.76

Table A.2. 387 mm standoff distance test data (English Units).

Point	Y-Coordinates (mm)	X-Coordinates (mm)	Scaled Distance (m/(kg^(1/3)))	0 mm Wall Height, 1219 mm Standoff Distance Pressure (Pa)	73 mm Wall Height, 1219 mm Standoff Distance Pressure (Pa)	226 mm Wall Height, 1219 mm Standoff Distance Pressure (Pa)
8	0.0	84.1	2.42	94,617	494,745	39,893
18	230.2	96.8	7.19	83,070	450,196	31,874
20	174.6	177.8	7.17	81,408	481,054	36,703
22	96.8	231.8	7.23	79,138	385,093	40,941
24	0.0	249.2	7.18	80,287	349,086	41,706
26	-96.8	231.8	7.23	87,775	349,580	36,241
28	-174.6	177.8	7.17	85,555	476,688	36,735
30	-230.2	96.8	7.19	92,590	442,163	31,210
35	484.2	120.7	14.37	77,082	340,711	33,433
37	415.9	279.4	14.42	57,952	251,314	42,938
39	277.8	414.3	14.36	58,762	205,818	43,481
42	0.0	498.5	14.35	56,526	187,361	49,672
45	-277.8	414.3	14.36	58,633	206,831	44,800
47	-415.9	279.4	14.42	64,650	234,985	36,588
49	-484.2	120.7	14.37	79,563	331,089	31,082
53	992.2	103.2	28.72	57,078	132,777	28,767
55	927.1	382.6	28.87	47,091	102,881	37,409
57	708.0	706.4	28.79	38,414	81,806	39,925
59	385.8	925.5	28.87	37,089	74,411	37,937
61	0.0	1000.1	28.79	40,608	88,742	39,964
63	-385.8	925.5	28.87	36,126	82,675	37,818
65	-708.0	706.4	28.79	37,048	91,436	39,183
67	-927.1	382.6	28.87	44,896	102,755	37,884
69	-992.2	103.2	28.72	59,366	139,713	28,075
72	1741.5	181.0	50.41	34,601	51,021	22,872
74	1619.3	671.5	50.47	31,873	50,748	33,699
76	1238.3	1238.3	50.41	25,859	39,231	26,014
78	669.9	1617.7	50.41	21,836	38,857	25,389
80	0.0	1751.0	50.41	23,985	33,931	24,545
82	-669.9	1617.7	50.41	23,796	40,307	25,396
84	-1238.3	1238.3	50.41	24,557	40,608	26,690
86	-1619.3	671.5	50.47	28,089	47,712	32,102
88	-1741.5	181.0	50.41	34,396	52,986	22,732
90	2498.7	84.1	71.98	24,440	30,123	18,067
92	2438.4	606.4	72.34	20,967	28,388	24,208
94	2076.5	1387.5	71.90	19,521	30,332	21,530
96	1387.5	2079.6	71.97	18,207	27,345	18,602
99	-1387.5	2079.6	71.97	20,595	31,408	18,984
101	-2076.5	1387.5	71.90	17,122	28,652	18,705
103	-2438.4	606.4	72.34	21,112	25,825	24,141
105	-2498.7	84.1	71.98	25,559	32,054	19,760
107	2703.5	1822.5	93.86	13,981	19,124	14,631
108	2298.7	2300.3	93.62	20,648	31,560	18,446
109	-2298.7	2300.3	93.62	13,079	18,172	12,955
110	-2703.5	1822.5	93.86	17,634	19,974	14,633

Table A.3. 1219 mm standoff distance test data (Metric Units).

Point	Y-Coordinates (in)	X-Coordinates (in)	Scaled Distance (ft/(lb^(1/3)))	0 mm Wall Height, 1219 mm Standoff Distance Pressure (psi)	73 mm Wall Height, 1219 mm Standoff Distance Pressure (psi)	226 mm Wall Height, 1219 mm Standoff Distance Pressure (psi)
8	0.0	3.3	6.09	13.72	71.76	5.79
18	9.1	3.8	18.08	12.05	65.30	4.62
20	6.9	7.0	18.04	11.81	69.77	5.32
22	3.8	9.1	18.18	11.48	55.85	5.94
24	0.0	9.8	18.04	11.64	50.63	6.05
26	-3.8	9.1	18.18	12.73	50.70	5.26
28	-6.9	7.0	18.04	12.41	69.14	5.33
30	-9.1	3.8	18.08	13.43	64.13	4.53
35	19.1	4.8	36.12	11.18	49.42	4.85
37	16.4	11.0	36.27	8.41	36.45	6.23
39	10.9	16.3	36.11	8.52	29.85	6.31
42	0.0	19.6	36.08	8.20	27.17	7.20
45	-10.9	16.3	36.11	8.50	30.00	6.50
47	-16.4	11.0	36.27	9.38	34.08	5.31
49	-19.1	4.8	36.12	11.54	48.02	4.51
53	39.1	4.1	72.20	8.28	19.26	4.17
55	36.5	15.1	72.59	6.83	14.92	5.43
57	27.9	27.8	72.39	5.57	11.87	5.79
59	15.2	36.4	72.57	5.38	10.79	5.50
61	0.0	39.4	72.39	5.89	12.87	5.80
63	-15.2	36.4	72.57	5.24	11.99	5.49
65	-27.9	27.8	72.39	5.37	13.26	5.68
67	-36.5	15.1	72.59	6.51	14.90	5.49
69	-39.1	4.1	72.20	8.61	20.26	4.07
72	68.6	7.1	126.73	5.02	7.40	3.32
74	63.8	26.4	126.88	4.62	7.36	4.89
76	48.8	48.8	126.75	3.75	5.69	3.77
78	26.4	63.7	126.73	3.17	5.64	3.68
80	0.0	68.9	126.74	3.48	4.92	3.56
82	-26.4	63.7	126.73	3.45	5.85	3.68
84	-48.8	48.8	126.75	3.56	5.89	3.87
86	-63.8	26.4	126.88	4.07	6.92	4.66
88	-68.6	7.1	126.73	4.99	7.69	3.30
90	98.4	3.3	180.96	3.54	4.37	2.62
92	96.0	23.9	181.87	3.04	4.12	3.51
94	81.8	54.6	180.76	2.83	4.40	3.12
96	54.6	81.9	180.95	2.64	3.97	2.70
99	-54.6	81.9	180.95	2.99	4.56	2.75
101	-81.8	54.6	180.76	2.48	4.16	2.71
103	-96.0	23.9	181.87	3.06	3.75	3.50
105	-98.4	3.3	180.96	3.71	4.65	2.87
107	106.4	71.8	235.99	2.03	2.77	2.12
108	90.5	90.6	235.38	2.99	4.58	2.68
109	-90.5	90.6	235.38	1.90	2.64	1.88
110	-106.4	71.8	235.99	2.56	2.90	2.12

Table A.4. 1219 mm standoff distance test data (English Units).

Point	Y-Coordinates (mm)	X-Coordinates (mm)	Scaled Distance (m/(kg^(1/3)))	0 mm Wall Height, 2046 mm Standoff Distance Pressure (Pa)	73 mm Wall Height, 2046 mm Standoff Distance Pressure (Pa)	226 mm Wall Height, 2046 mm Standoff Distance Pressure (Pa)
8	0.0	84.1	2.42	37,498	62,811	18,161
18	230.2	96.8	7.19	35,692	64,928	15,453
20	174.6	177.8	7.17	36,738	76,975	16,683
22	96.8	231.8	7.23	33,226	75,385	18,735
24	0.0	249.2	7.18	35,588	76,428	18,352
26	-96.8	231.8	7.23	39,038	82,390	19,193
28	-174.6	177.8	7.17	38,990	84,477	18,508
30	-230.2	96.8	7.19	38,369	63,533	15,014
35	484.2	120.7	14.37	36,214	64,820	16,892
37	415.9	279.4	14.42	29,822	63,441	19,429
39	277.8	414.3	14.36	28,078	58,279	19,563
42	0.0	498.5	14.35	27,882	55,710	20,606
45	-277.8	414.3	14.36	30,551	60,855	19,117
47	-415.9	279.4	14.42	35,067	62,924	15,534
49	-484.2	120.7	14.37	35,202	63,280	12,601
53	992.2	103.2	28.72	30,440	48,826	15,263
55	927.1	382.6	28.87	26,915	50,541	15,904
57	708.0	706.4	28.79	23,394	40,727	22,649
59	385.8	925.5	28.87	20,675	36,044	22,872
61	0.0	1000.1	28.79	24,394	40,231	24,033
63	-385.8	925.5	28.87	21,707	36,586	22,068
65	-708.0	706.4	28.79	25,812	37,535	19,597
67	-927.1	382.6	28.87	26,395	50,021	16,196
69	-992.2	103.2	28.72	32,697	48,107	12,542
72	1741.5	181.0	50.41	23,346	37,324	13,714
74	1619.3	671.5	50.47	20,744	33,446	16,518
76	1238.3	1238.3	50.41	17,343	26,697	18,480
78	669.9	1617.7	50.41	16,547	23,114	16,345
80	0.0	1751.0	50.41	16,382	24,610	16,934
82	-669.9	1617.7	50.41	15,984	22,739	17,726
84	-1238.3	1238.3	50.41	18,278	26,924	19,602
86	-1619.3	671.5	50.47	19,864	31,362	18,954
88	-1741.5	181.0	50.41	23,424	38,608	13,757
90	2498.7	84.1	71.98	18,685	23,185	13,544
92	2438.4	606.4	72.34	16,320	22,976	15,279
94	2076.5	1387.5	71.90	13,298	19,135	17,046
96	1387.5	2079.6	71.97	12,755	18,535	13,654
99	-1387.5	2079.6	71.97	15,601	20,413	15,440
101	-2076.5	1387.5	71.90	13,633	19,547	14,463
103	-2438.4	606.4	72.34	16,515	23,493	14,817
105	-2498.7	84.1	71.98	20,491	24,538	11,944
107	2703.5	1822.5	93.86	12,008	13,511	12,905
108	2298.7	2300.3	93.62	12,705	21,698	13,592
109	-2298.7	2300.3	93.62	10,469	13,585	10,664
110	-2703.5	1822.5	93.86	13,534	18,099	9,411

Table A.5. 2046 mm standoff distance test data (Metric Units).

Point	Y-Coordinates (in)	X-Coordinates (in)	Scaled Distance (ft/(lb^(1/3)))	0 mm Wall Height, 2046 mm Standoff Distance Pressure (psi)	73 mm Wall Height, 2046 mm Standoff Distance Pressure (psi)	226 mm Wall Height, 2046 mm Standoff Distance Pressure (psi)
8	0.0	3.3	6.09	5.44	9.11	2.63
18	9.1	3.8	18.08	5.18	9.42	2.24
20	6.9	7.0	18.04	5.33	11.16	2.42
22	3.8	9.1	18.18	4.82	10.93	2.72
24	0.0	9.8	18.04	5.16	11.09	2.66
26	-3.8	9.1	18.18	5.66	11.95	2.78
28	-6.9	7.0	18.04	5.66	12.25	2.68
30	-9.1	3.8	18.08	5.57	9.21	2.18
35	19.1	4.8	36.12	5.25	9.40	2.45
37	16.4	11.0	36.27	4.33	9.20	2.82
39	10.9	16.3	36.11	4.07	8.45	2.84
42	0.0	19.6	36.08	4.04	8.08	2.99
45	-10.9	16.3	36.11	4.43	8.83	2.77
47	-16.4	11.0	36.27	5.09	9.13	2.25
49	-19.1	4.8	36.12	5.11	9.18	1.83
53	39.1	4.1	72.20	4.42	7.08	2.21
55	36.5	15.1	72.59	3.90	7.33	2.31
57	27.9	27.8	72.39	3.39	5.91	3.29
59	15.2	36.4	72.57	3.00	5.23	3.32
61	0.0	39.4	72.39	3.54	5.84	3.49
63	-15.2	36.4	72.57	3.15	5.31	3.20
65	-27.9	27.8	72.39	3.74	5.44	2.84
67	-36.5	15.1	72.59	3.83	7.26	2.35
69	-39.1	4.1	72.20	4.74	6.98	1.82
72	68.6	7.1	126.73	3.39	5.41	1.99
74	63.8	26.4	126.88	3.01	4.85	2.40
76	48.8	48.8	126.75	2.52	3.87	2.68
78	26.4	63.7	126.73	2.40	3.35	2.37
80	0.0	68.9	126.74	2.38	3.57	2.46
82	-26.4	63.7	126.73	2.32	3.30	2.57
84	-48.8	48.8	126.75	2.65	3.91	2.84
86	-63.8	26.4	126.88	2.88	4.55	2.75
88	-68.6	7.1	126.73	3.40	5.60	2.00
90	98.4	3.3	180.96	2.71	3.36	1.96
92	96.0	23.9	181.87	2.37	3.33	2.22
94	81.8	54.6	180.76	1.93	2.78	2.47
96	54.6	81.9	180.95	1.85	2.69	1.98
99	-54.6	81.9	180.95	2.26	2.96	2.24
101	-81.8	54.6	180.76	1.98	2.84	2.10
103	-96.0	23.9	181.87	2.40	3.41	2.15
105	-98.4	3.3	180.96	2.97	3.56	1.73
107	106.4	71.8	235.99	1.74	1.96	1.87
108	90.5	90.6	235.38	1.84	3.15	1.97
109	-90.5	90.6	235.38	1.52	1.97	1.55
110	-106.4	71.8	235.99	1.96	2.63	1.37

Table A.6. 2046 mm standoff distance test data (English Units).

WORKS CITED

"Blast Effects Computer Version 5.0." 2001. Department of Defense Explosives Safety Board. Alexandria, VA.

Cooper, Paul W. 1996. *Explosives Engineering*. Wiley-VCH, Inc, New York, NY.

Johansson, C.H. and Persson, P.A. 1970. *Detonics of High Explosives*. Academic Press, London.

Remennikov, Alex M. and Rose, Timothy A. 2007. "Predicting the Effectiveness of Blast Wall Barriers Using Neural Networks." International Journal of Impact Engineering 34: 1907-1923.

Rickman, Dennis D. and Murrell, Donald W. 2004. "Miniature-Scale Experiments of Airblast Diffraction Over Barrier Walls: Results and Analysis." ERDC/GSL ; TR-04-2.

Smith, Peter D. and Hetherington, John G. 1994. *Blast and Ballistic Loading of Structures*. Butterworth-Heinemann, Oxford.

TM 1300. 1990. "Structures to Resist the Effects of Accidental Explosions." U.S. Dept. of Army Technical Manual, Washington, D.C.

TM 5-853-3. 2005. "Security Engineering Final Design." U.S. Dept. of Army Technical Manual, Washington, D.C.

TM 5-855-1. 1987. "Fundamentals of Protective Design for Conventional Weapons." U.S. Dept. of Army Technical Manual, Washington, D.C.

Walter, Patrick L. 2004. "Introduction to Air Blast Measurement Parts I-V." PCB Piezotronics, Depew, NY.

Zhou, X.Q. and Hao, H. 2006. "Prediction of Airblast Loads on Structures Behind a Protective Barrier." International Journal of Impact Engineering 35: 363-375.

Zipf, R.K. and Cashdollar, K.L. 2007. "Explosions and Refuge Chambers," NIOSH Docket Number 125. National Institute for Occupational Safety and Health, Columbus, OH.

VITA

Nathan Thomas Rouse was born in Carthage, Illinois. He completed his Bachelor of Science in Mining Engineering at the University of Missouri-Rolla in 2009 and will receive his Master of Science in Explosives Engineering at Missouri S&T in 2010. He has worked for Arch Coal as a mining engineering intern and for Schlumberger Reservoir Completions as an explosives engineering intern. Nathan is currently employed as a mining engineer by Morgan Worldwide Consultants in Lexington, KY.